Journal of
Medicinal Chemistry

Article

Subtype-selective Fluorescent Ligands as Pharmacological Research Tools for the Human Adenosine A2A Receptor

Eleonora Comeo, Nicholas D. Kindon, Mark Soave, Leigh A. Stoddart, Laura Kilpatrick, Peter J. Scammells, Stephen John Hill, and Barrie Kellam

J. Med. Chem., **Just Accepted Manuscript** • DOI: 10.1021/acs.jmedchem.9b01856 • Publication Date (Web): 30 Dec 2019

Just Accepted

is published by the American Chemical Society. 1155 Sixteenth Street N.W., Washington, DC 20036

Subtype-selective Fluorescent Ligands as Pharmacological Research Tools for the Human Adenosine A_{2A} Receptor.

Eleonora Comeo[1,3,4]; Nicholas D. Kindon[1,3]: Mark Soave[2,3]; Leigh A. Stoddart[2,3]; Laura E. Kilpatrick[2,3]; Peter J. Scammells[4]; Stephen J. Hill[2,3] and Barrie Kellam[1,3 *].*

[1] Division of Biomolecular Sciences and Medicinal Chemistry, School of Pharmacy, Centre for Biomolecular Sciences, University of Nottingham, NG7 2RD, UK.

[2] Division of Physiology, Pharmacology and Neuroscience, School of Life Sciences, University of Nottingham, NG7 2UH, UK.

[3] Centre of Membrane Proteins and Receptors (COMPARE) University of Birmingham and University of Nottingham, The Midlands, NG7 2UH, UK.

[4] Medicinal Chemistry, Monash Institute of Pharmaceutical Sciences, Monash University, 381 Royal Parade, Parkville, Victoria 3052 Australia

KEYWORDS: Adenosine A_{2A} receptor, fluorescent antagonist, BODIPY, GPCR, NanoBRET, preladenant, imaging, FRET

ABSTRACT

Among class A G protein-coupled receptors (GPCR), the human adenosine A_{2A} receptor ($hA_{2A}AR$) remains an attractive drug target. However, translation of $A_{2A}AR$ ligands into the clinic has proved challenging and an improved understanding of $A_{2A}AR$ pharmacology could promote development of more efficacious therapies. Subtype-selective fluorescent probes would allow detailed real-time pharmacological investigations both in vitro and in vivo. In the present study, two families of fluorescent probes were designed around the known $hA_{2A}AR$ selective antagonist preladenant (SCH 420814). Both families of fluorescent antagonists retained affinity at the $hA_{2A}AR$, selectivity over all other adenosine receptor subtypes and allowed clear visualization of specific receptor localization through confocal imaging. Furthermore, the AlexaFluor647-labelled conjugate allowed measurement of ligand binding affinities of unlabeled $hA_{2A}AR$ antagonists using a bioluminescence resonance energy transfer (NanoBRET) assay. The fluorescent ligands developed here can therefore be applied to a range of fluorescence-based techniques to further interrogate $hA_{2A}AR$ pharmacology and signaling.

INTRODUCTION

The adenosine receptors belong to class A of the G protein-coupled receptor (GPCR) superfamily with the latter accounting for about 30% of the molecular targets for currently marketed drugs.[1] The pharmacological profile of the adenosine receptors is defined by the function of four adenosine receptor subtypes- A_1, A_{2A}, A_{2B} and A_3 - each of which possess distinct signaling and pharmacological properties[2]. Among this family, the adenosine A_{2A} receptor ($A_{2A}AR$) represents an attractive drug target which has been the subject of intensive medicinal chemistry research over the last forty years.[3,4] The $A_{2A}ARs$ signal primarily through

$G\alpha_S$ proteins in the periphery[2] but can also signal through $G\alpha_{olf}$ in the striatum.[5] Upon receptor activation, both G_s and G_{olf}-coupled receptors act by stimulating adenylyl cyclase leading to an increase of intracellular cAMP levels, and subsequent activation of a series of downstream signaling cascades.[6] Over thirty X-ray crystal structures for the $hA_{2A}AR$ have been solved in complex with a range of molecules, providing useful insights into the structural framework of this membrane protein and helped the rational design and development of selective $hA_{2A}AR$ ligands[7–11] for the treatment of several diseases including cardiovascular, inflammatory and CNS disorders.[12–14] More recently blockade of the $A_{2A}AR$ pathway has generated renewed interest because of the role of adenosinergic signaling in cancer immunotherapy.[15] In vitro studies and animal models have shown that adenosine-mediated activation of the high affinity $A_{2A}ARs$ expressed on the surface of immune cells suppresses the anti-tumor response in the host, facilitating cancer growth and dissemination.[16,17] Moreover, the expression of $A_{2A}ARs$ correlates with the malignancy of the tumor, suggesting these membrane-bound proteins might be considered as a prognostic biomarker for the severity of neoplastic disease.[18] A number of small-molecule $A_{2A}AR$ antagonists are currently being explored as novel therapeutics to inhibit this adenosine-mediated suppression of the immune responses in patients with solid malignancies, including non-small cell lung cancer, breast cancer and prostate carcinoma (Figure 1).

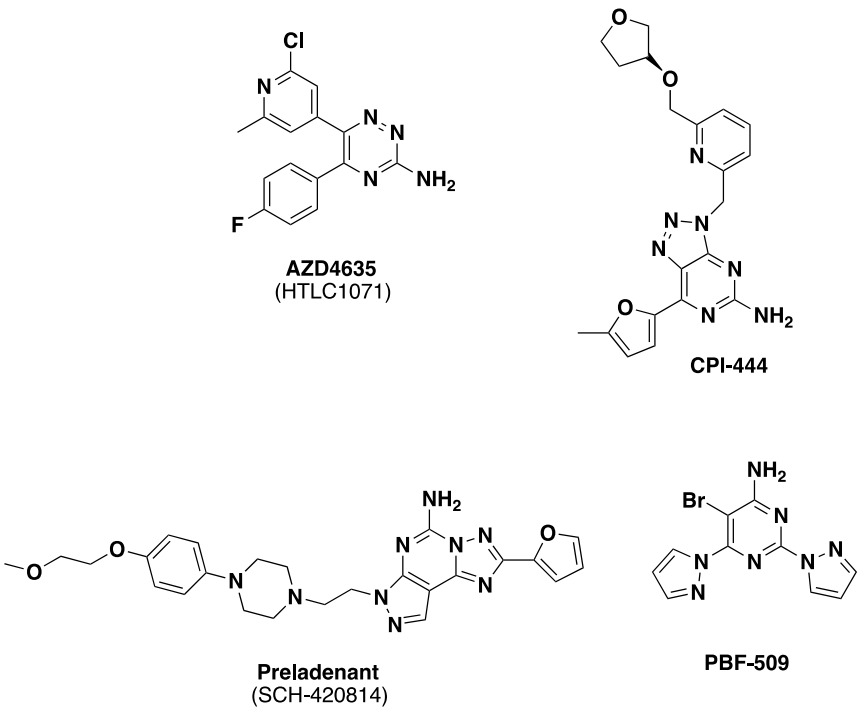

Figure 1. Small molecule $hA_{2A}AR$ antagonists currently investigated as single agents, or in combination with monoclonal antibodies, in patients with solid tumors.

To date only two molecules targeting the $A_{2A}AR$ have reached the market: Regadenoson (Lexiscan, Astellas Pharma) a pharmacological stress agent for myocardial perfusion injury[12,19] and Istradefylline (NOURIANZ®, Kyowa Kirin Inc.), a xanthine-based $hA_{2A}AR$ antagonist which has reached the market in Japan for treating the symptoms of Parkinson's Disease (PD)[20,21] However, despite the many therapeutic opportunities associated with the $A_{2A}AR$, translation of adenosine ligands from the bench into the clinic has been hampered by a lack of understanding of the tissue and cell-type specific receptor pharmacology leading to on-target side effects.[13] Additional knowledge on the function of the $A_{2A}AR$ could be achieved through real-time monitoring of the localization and function of the receptor at native expression levels in specific human cell types in both health and disease, with the aim of developing more selective and efficacious therapies. Fluorescent ligands therefore represent useful tools to achieve this aim

as they offer the ability to study the target receptor at endogenous expression levels, in real-time and, importantly, in unmodified living cells.[22]

Fluorescent ligands for the ARs have been successfully developed and have allowed various aspects of their pharmacology, such as the signaling[23,24] and dynamics[25,26], to be investigated. For example, the BODIPY 630/650-X-labelled xanthine amine congener (XAC), developed in our laboratories, allowed the quantification of specific A_1AR-antagonist complexes at the single molecule level in living cells using fluorescence correlation spectroscopy (FCS).[26] However, intracellular accumulation of the ligand observed over extended incubation times through confocal microscopy, as well as the promiscuous nature of the probe in binding other adenosine receptors, restricted its use to recombinant cells. Receptor-subtype selectivity is particularly important when probing the A_{2A}AR pharmacology in unmodified, endogenously expressing tissues and cells, as other adenosine receptor subtypes are often co-expressed.[2,12] Jacobson and co-workers pioneered the development of fluorescent probes selective for the hA_{2A}AR, including fluorescent analogues of the A_{2A}AR selective antagonist SCH442416 labelled with an AlexaFluor488 dye, that have been used successfully for fluorescence polarization[27] and flow cytometry[28] assays. However, the utility of these probes for bioimaging studies has not yet been reported. This suggests there still remains the need to develop additional selective hA_{2A}AR probes, optimized for imaging studies that would allow specific visualization of the hA_{2A}AR at the single cell level in healthy and diseased systems.

In the present study, we sought to expand the current pharmacological toolkit for the hA_{2A}AR by generating a more versatile suite of fluorescent probes with regard to their photochemical and physicochemical properties and areas of potential application. Here we report the design, synthesis and pharmacological evaluation of a novel series of subtype-selective fluorescent

ligands (**12-17**) for the human adenosine $hA_{2A}AR$ receptor based upon preladenant (a high affinity ($hA_{2A}AR$ K_i = 1.0 nM)[29] and highly selective (hA_1, hA_{2B} and hA_3 K_i > 1000 nM)[29] $hA_{2A}AR$ antagonist) which are amenable to use in a variety of fluorescence-based techniques. These $A_{2A}AR$ selective fluorescent ligands will be valuable tools for the wider scientific community for both in vitro and in vivo applications and high-resolution imaging studies into the role of $A_{2A}AR$ in health and disease.

RESULTS AND DISCUSSION

Design Strategy. Our synthetic strategy commenced by exploring the existing structure-activity-relationships (SAR)[4,30–32] of the selected parent drug preladenant in binding to the $A_{2A}AR$ to identify the optimal position of the molecule that would be relatively insensitive to structural modifications and allow fluorophore attachment without affecting the original pharmacological properties of the ligand. This preliminary screening was complemented through in silico studies which were undertaken to rationalize the possible binding interactions established between the parent ligand and the $hA_{2A}AR$ (Figure 2).

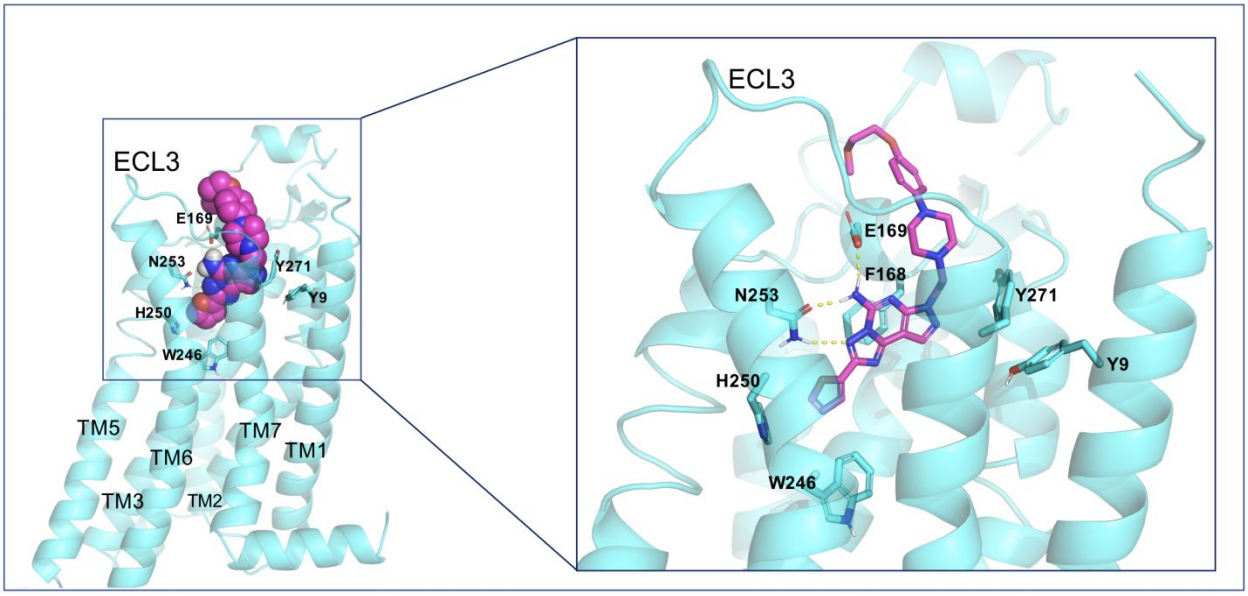

Figure 2. Molecular Docking of preladenant to the crystal structure of the $hA_{2a}AR$ (PDB=4EIY) executed with Schrödinger's Glide (Schrödinger release 2018-3). The images were generated with PyMOL (version 2.2.0). Preladenant is shown in spheres colored magenta. The GPCR is shown in ribbon colored cyan. The key residues are labelled and shown in sticks. A zoomed view of preladenant (shown in licorice) in the binding pocket is depicted in the box with hydrogen bonding interactions depicted as dashed lines.

Molecular docking simulations of preladenant to the 1.8 angstrom resolution crystal structure (PDB = 4EIY) of the $hA_{2A}AR$[9] revealed the core pyrazolo[4,3-*e*][1,2,3]triazolo[1,5-*c*]pyrimidin-5-amine (PTP) scaffold interacts with key receptor residues in an equivalent fashion to the antagonist ZM241385, including polar contacts with Asn253 and Glu169 and a π–stacking interaction with Phe168[7,9]. The side chain of preladenant adopted a conformation extending towards extracellular loop 3 (ECL3) and, therefore, to a more solvent-exposed region of the GPCR. These results were further validated by previously reported SAR studies which showed that modifications at the extended methoxyethylether moiety were well tolerated.[4,30,31,33] Thus, it seemed logical to exploit this side chain of preladenant as a flexible point to explore linker/fluorophore elaboration. We hypothesized that an amino alkyl spacer would provide

sufficient spatial separation between the fluorophore and the orthosteric binding moiety. When designing fluorescent probes the introduction of a spacer between the parent pharmacophore and the fluorophore is often included in the design strategy and the nature and the length of the linker and the fluorophore itself can significantly influence the final pharmacological profile of the fluorescent conjugate.[34,35] Structural modifications must be performed at specific positions which can be easily tolerated and do not cause significant impact upon pharmacological activity. Therefore, we undertook modification of the methoxy tail of the parent compound preladenant by conjugation with an amino alkyl spacer, leading to the corresponding amino functionalized congener amenable to conjugation with a series of commercially available fluorophores (Scheme 1). This novel series of fluorescent ligands included probes featuring the 4,4-difluoro-4-bora-3a,4a-diaza-s-indacene (BODIPY) dyes alongside water-soluble dyes such as sulfonated cyanine-5 (sulfo-Cy5) and AlexaFluor647 fluorophores. These probes were selected on the basis of several considerations. For example, the use of fluorophores with long-wavelength excitation/emission spectra is preferred as it minimizes the degree of overlap with background autofluorescence in living cells.[23,35–38] The BODIPY fluorophores embody the first choice for fluorescent derivatization given their stability and photochemical properties.[39] The 6-(((4,4-difluoro-5-(2-thienyl)-4-bora-3a,4a-diaza-s-indacene-3-yl)styryloxy)acetyl)aminohexanoic acid (BODIPY630/650) is often the favored among this family of dyes due to its advantageous spectral profile (excitation 630 nm, emission 650 nm). It has been previously suggested that given the lipophilic nature of the probe, the BODIPY moiety is likely to reside within the membrane bilayer. Indeed, this fluorophore has been shown to be heavily quenched in aqueous solution, therefore the optimal location would be in a lipid environment as this reduces background fluorescence from non-bound ligand which is particularly advantageous for imaging

studies.[34] However, the intrinsic lipophilic nature of these dyes may limit their applicability in vivo due to the reduced stability in the bloodstream as well as limited detection after IV administration.[40] One possible strategy to overcome these issues is by employing water-soluble fluorophores such as those belonging to the Cy5 and AlexaFluor families of dyes. These water-soluble dyes also possess good photochemical properties and have therefore been particularly advantageous for the development of in vivo probes such as in cancer imaging.[41]

Synthesis of the Fluorescent $hA_{2A}AR$ Antagonists. Based on the information obtained from the molecular docking studies, a novel series of fluorescent antagonists for the $hA_{2A}AR$ receptor were synthesized featuring BODIPY-, Cy5- and AF647-based probes. The general route to the desired probes is illustrated in Scheme 1.

The synthesis comprised ten steps to a common precursor from which six different fluorescent analogues were generated. Firstly, a one pot procedure reported by Kuo et al.[42] for the synthesis of intermediate **4** was followed. This involved reaction of commercially available 2-amino-4,6-diclhoropyrimidine-5-carbaldehyde (**1**) with 2-furoic hydrazide in anhydrous THF in the presence of Et_3N under reflux for 2h to obtain **2** via nucleophilic aromatic substitution (S_NAr). Once the desired product was formed, solvent was removed in vacuo and a solution of 2-hydroxyethylhydrazine in a mixture of CH_3CN/H_2O was added to the crude product to displace the chlorine at the 2-position through S_NAr and afforded compound **3** after ring rearrangement. Thereafter, **3** was cyclised in the presence of a catalytic amount of $ZnBr_2$ and an excess of $POCl_3$.

Scheme 1. Synthesis of the Fluorescent hA_{2A} AR Antagonists [a].

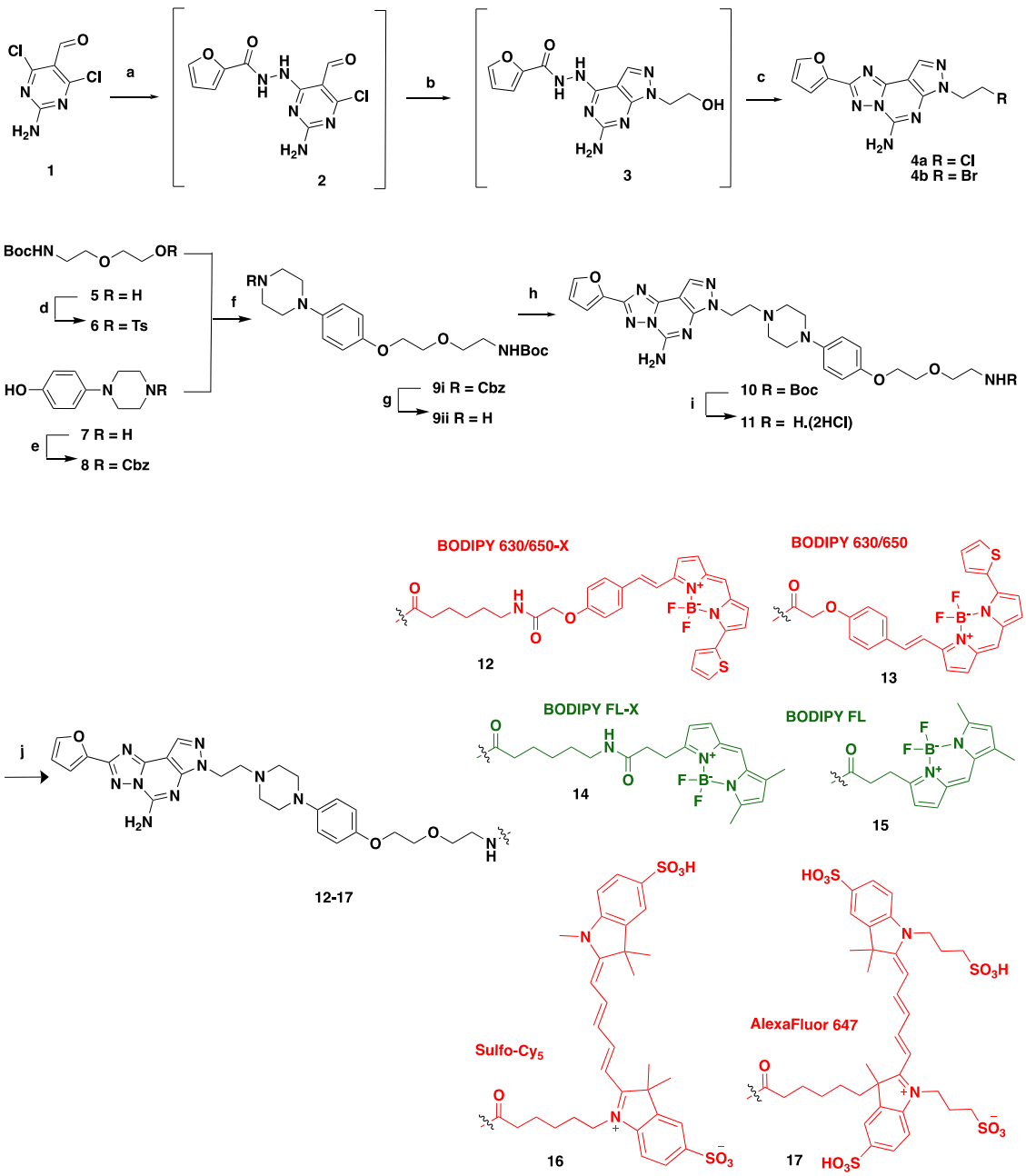

[a] Reagents and conditions a) 2-furoic hydrazide, NEt_3, dry THF, reflux b) 2- hydroxyethylhydrazine, CH_3CN/H_2O, reflux c) $POCl_3$, $ZnBr_2$, 80°C for 5h, 11% over three steps d) TsCl, DIPEA, DMAP 5%mol, DCM, 86% e) CbzCl, K_2CO_3, DMF, 66% f) K_2CO_3, CH_3CN, 100°C for 6h, 40% g) H_2, Pd/C, EtOH, 82% h) **4**, DIPEA, DMF, 80°C, 20% i) 4N HCl in dioxane, RT, quantitative j) 12-14-15-16-17 Fluorophore-NHS, DIPEA, DMF, RT,97% -quantitative; **13** BODIPY carboxylic acid, HATU, DIPEA, DMF, 96%.

This dehydrative cyclization occurred with concomitant Dimroth rearrangement[44] to afford intermediate **4** in a disappointing overall yield (11% over three steps). Mass spectroscopy and ^1H

NMR showed that the desired product afforded was a 2:1 mixture of chloride and bromide derivatives: one single peak at t_R=2.50, $M+H^+$ = 304 (**4$_a$**) and $M+H^+$ = 348 (**4$_b$**); in the ^{1}H NMR analysis the peaks characteristic of the aromatic region of the spectra were in common to both. Conversely, the peaks characteristic of the alkyl halide tail appeared in the spectra with different chemical shifts for both bromide and chloride derivatives: peaks at 4.66 ppm (t, *J*=6.2 Hz, 1H, -C$\underline{H}_2$Br), 4.60 ppm (t, *J*=5.9 Hz, 2H, -C$\underline{H}_2$Cl), 4.09 ppm (t, *J*=5.9 Hz, 2H, -C$\underline{H}_2$CH$_2$Cl), 3.94 ppm (t, *J*=6.2 Hz, 1H, -C$\underline{H}_2$CH$_2$Br).

Subsequently, synthesis of the amino functionalized tail of the final molecule started by activating the hydroxyl group of commercially available **5** with tosyl chloride in DCM to afford **6**. Under basic conditions, commercially available 1-(4-hydroxyphenyl) piperazine **7** was protected at the free secondary amino group with benzyl chloroformate to afford the corresponding benzylcarbamate-protected piperazine derivative **8** with reasonable yield (66%). Under basic conditions, nucleophilic displacement of the tosyl group of **6** by the phenolic hydroxyl of **8** afforded the di-protected intermediate **9**. This allowed selective removal of the two protecting groups employing different conditions: hydrogenolysis of the benzylcarbamate group in the presence of 10% palladium-on-carbon (Pd/C) gave the corresponding free secondary amine in quantitative yield. Under basic conditions, substitution of the primary ethyl halide tail of compound **4** by the nucleophilic piperazine nitrogen afforded compound **10** which underwent acidolytic Boc deprotection to generate the corresponding amine **11** as its di-HCl salt. Finally, **11** was coupled with the appropriate commercially available BODIPY, Cy5 and AF647 succinimidyl esters and to a BODIPY 630/650 carboxylic acid (**13**) synthesized in our laboratory[45] to afford a focused library of six fluorescent analogues (**12-17**).

The novel fluorescent conjugates were isolated and purified by reverse-phase high performance liquid chromatography (RP-HPLC). The final purity of the fluorescent ligands was confirmed by analytical RP-HPLC with dual wavelength detection and were determined as being ≥ 96% homogenous. Additionally, the chemical identity of probes (**12-17**) was confirmed by High Resolution Mass Spectrometry (HRMS) (TOF ES+ and ES-).

Pharmacological Evaluation of the Fluorescent hA_{2A}AR Antagonists. The novel preladenant-based fluorescent ligands were assessed in a variety of pharmacological assays. Firstly, the novel compounds were validated through a Bioluminescence Resonance Energy Transfer (BRET)[46,47] ligand binding assay, a proximity assay (<10 nm) that exploits the energy transfer between the donor bioluminescent protein nanoluciferase (NanoLuc)[48] tagged to the receptor of interest at its *N*-terminus (Nluc-A_{2A}AR) and an acceptor fluorescent molecule. For all of the fluorescent ligands used in the present study, a clear saturable component of specific binding could be detected (Table 1 and Figure 3) to the hA_{2A}AR that was associated with low levels of non-specific binding across all of the concentrations of fluorescent ligands measured.

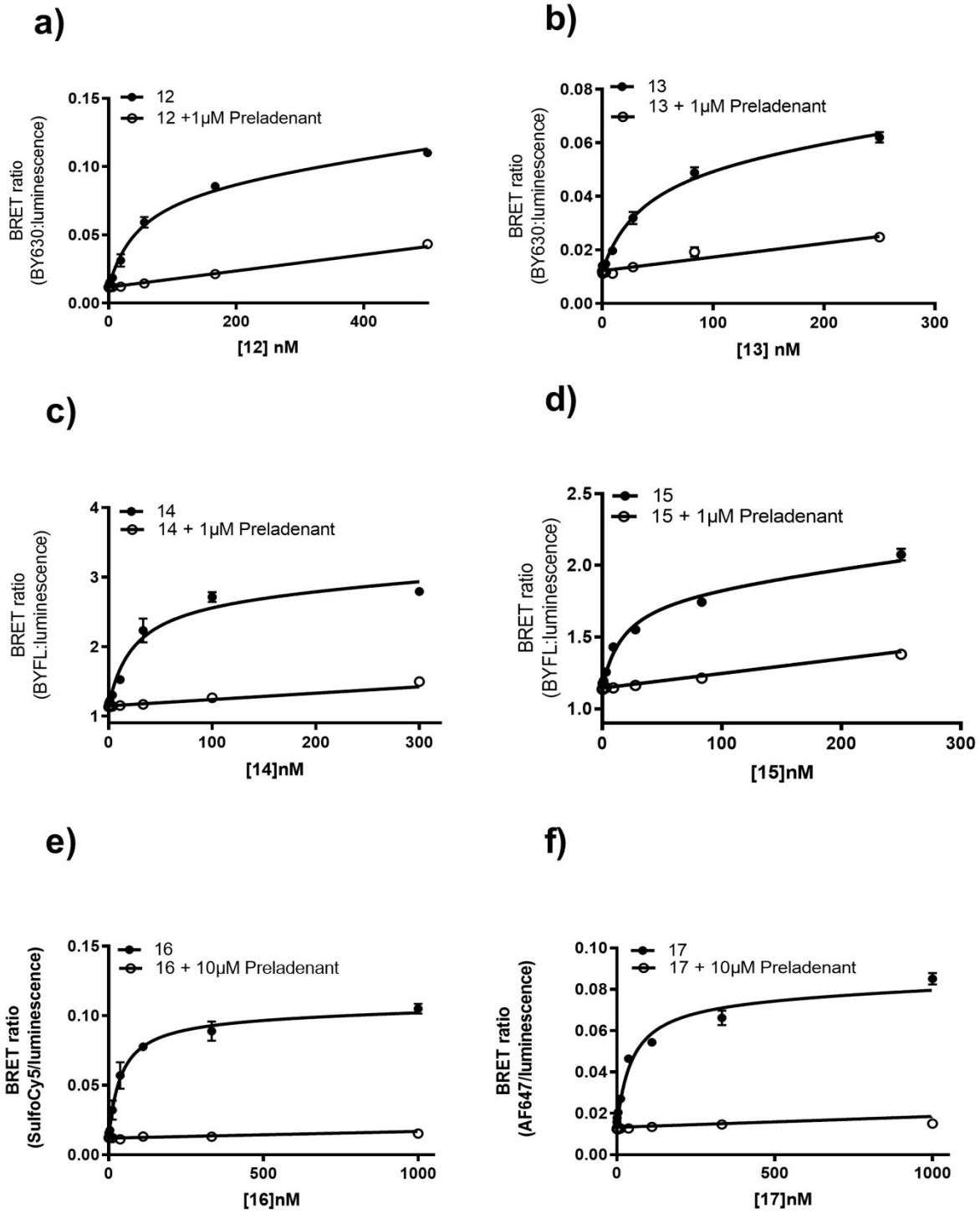

Figure 3. NanoBRET saturation binding curves measured in HEK293G cells transiently expressing the NanoLuc- hA$_{2A}$AR for a) **12,** b) **13**, c) **14**, d) **15,** e) **16** and f) **17** in the presence (open circles) and absence (closed circles) of 1μM preladenant. The graphs depicted are

representative of $n = 5$ (a, d, e and f) or $n = 4$ (b and c) separate experiments. Each data point represents the mean value ± SEM performed in triplicate in a single experiment.

The novel fluorescent conjugates were able to bind to the $hA_{2A}AR$ with good affinity. However, the affinity values measured for the water-soluble probes were slightly lower than the BODIPY conjugates (Table 1). A possible explanation of the differences in binding affinity values among the two groups of fluorescent ligands could be attributed to the fluorophores employed, considering they constituted the only structural difference between the compounds. It is possible that the boron dipyrromethene scaffold of the BODIPY-labelled $hA_{2A}AR$ fluorescent antagonists engages in a cooperative fashion with key residues in an additional pocket of the receptor[28], thereby contributing to increase the binding affinity of the ligands. Conversely, due to the more hydrophilic nature of the cyanine5 and AF647-bearing probes it is possible that these dyes are likely to be extending towards the extracellular medium without engaging to key residues. This hypothesis is consistent with previous work from our laboratories in which it has been demonstrated that the selective A_3 fluorescent conjugate bearing a Cy5 moiety displayed 300-fold lower affinity compared to the corresponding BODIPY630/650 conjugate with the same pharmacophore and linker, suggesting that the BODIPY fluorophores directly contribute in enhancing the binding affinity of ligands.[23,28,35]

Differences in the BRET ratio observed can be attributed to a variety of factors (Figure 3). For example, when using green-emitting ligands (excitation 503 nm, emission 512 nm) a greater contribution from the NanoLuc emission spectra (emission peak 462 nm) is detected in the green acceptor emission channel (535 nm), leading to an increase in the BRET ratio. Conversely, with red-shifted ligands the contribution of the NanoLuc emission is markedly reduced in the red acceptor channel and this leads to a reduction in the background BRET ratio.[46] The distance and

the specific orientation of the acceptor fluorophore with respect to the donor NanoLuc can also influence the efficiency of the energy transfer between the two species and contribute to the absolute differences in the BRET ratio observed[49].

Table 1. Binding Affinities of the novel Fluorescent Ligands determined in whole HEK293G cells transiently expressing the NanoLuc-*h*A_{2A}AR.

Compound	pK_D (LogM)[a]	n
12 (BY630/650-X)	7.39 ± 0.05	5
13 (BY630/650)	7.39 ± 0.02	4
14 (BY-FL-X)	7.77 ± 0.06	4
15 (BY-FL)	7.65 ± 0.10	5
16 (Sulfo-Cy5)	7.08 ± 0.09	5
17 (AF647)	7.22 ± 0.05	5

[a]pK_D value was calculated from the negative logarithm of the equilibrium dissociation constant (K_D) determined from saturation ligand binding assay using increasing concentration of labelled ligand in the absence or presence (to determine non-specific binding) of unlabeled ligand preladenant (1μM). Data are expressed as mean ± SEM of *n* experiments, where each experiment was performed in triplicate.

Achieving A_{2A}AR selectivity represents one of the major objectives of our study, especially when the fluorescent ligands are being developed with the intention of being applied to a variety of fluorescence-based techniques in different tissues and animal models endogenously expressing other adenosine receptor subtypes. The NanoBRET saturation ligand binding assay allowed us to determine the binding affinity of each fluorescent A_{2A}AR antagonist in HEK293 cells stably expressing either the NanoLuc-A_1, NanoLuc-A_{2B} or the NanoLuc-A_3 ARs. The

results revealed that no specific binding of the fluorescent ligands was detectable at the A_1, A_{2B} and A_3AR subtypes at concentrations tested (Figure 4).

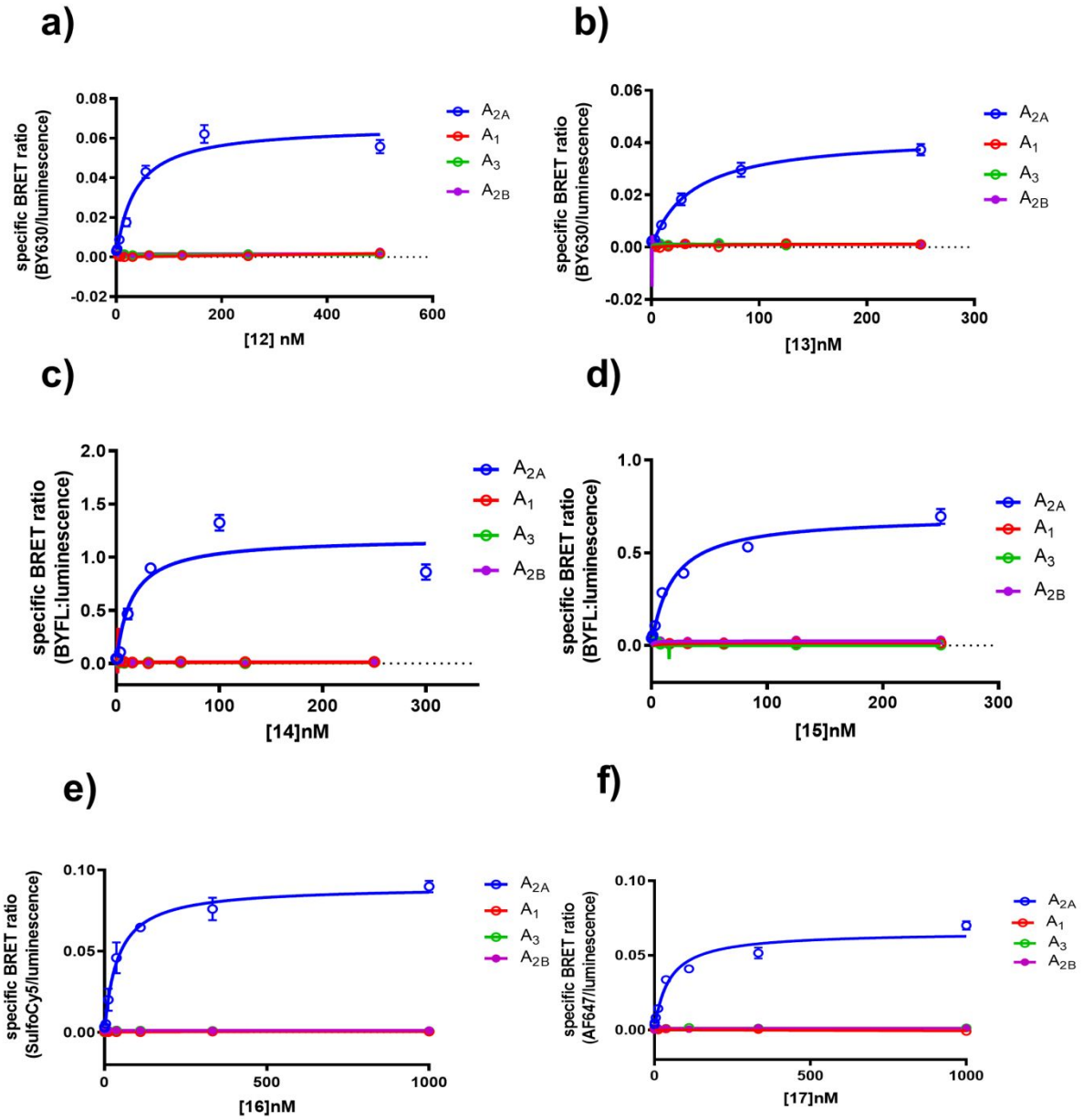

Figure 4. Specific binding of the novel fluorescent ligands at each subtype of adenosine receptor. The selectivity profiling of compound **12** a), **13** b), **14** c), **15** d), **16** e) and **17** f) is depicted by showing only the specific binding at each adenosine receptor subtype. For each compound the specific binding at each adenosine receptor was obtained by subtracting the non-specific binding component from the total binding derived from saturation binding experiments

(see Figure 1 and Table 1). Non-specific binding was defined in the presence of 1 μM preladenant for NanoLuc-A_{2A}AR, 10 μM DPCPX for NanoLuc-A_1, 10 μM MRS1220 for NanoLuc-A_3 and 10 μM PSB603 for NanoLuc-A_{2B}, respectively. The graphs shown above are representative of *n*=4 (c and d) and *n*=5 (a, b, e and f) experiments and the data are mean ± SEM of triplicate determinations in a single representative experiment.

Given the higher affinity displayed at the A_{2A}AR, the BODIPY-labelled ligands were selected to assess whether the novel synthesized probes were able to retain the functional antagonistic ability of the parent compound preladenant. This was performed using a previously described CRE-SPAP reporter gene assay[50] in CHO cells expressing the human adenosine hA_{2A}AR receptors. All the BODIPY-labelled ligands were able to inhibit adenosine-5-*N*-ethylcarboxamide (NECA)-mediated increase in SPAP production in a competitive fashion, causing a rightward shift of the NECA response curve as shown in Figure 5. From these data, it was possible to perform Schild regression analysis and estimate the affinity of each compound as shown in Table 2**.**

Table 2. pA_2 values of the BODIPY-labeled Fluorescent Ligands.

compound	***h*A_{2A}AR pA_2 [a]**	**n**
12 (BY630/650-X)	9.31± 0.38*†	7
13 (BY630/650)	8.61± 0.30	6
14 (BY-FL-X)	7.91± 0.26*	5
15 (BY-FL)	8.40± 0.26†	6

[a] Affinity of the BODIPY-labelled Fluorescent Ligands. Ability for these ligands to inhibit the NECA-stimulated CRE-SPAP response in CHO cells expressing the *h*A_{2A}AR. Data are mean ± SEM for *n* separate experiments performed in triplicate (statistical significance was defined as *p < 0.05 unpaired t-test comparing **12** and **14.** † p < 0.05 unpaired t-test comparing the binding affinity of **12** and **15** measured in CRE-SPAP assay and the NanoBRET assay).

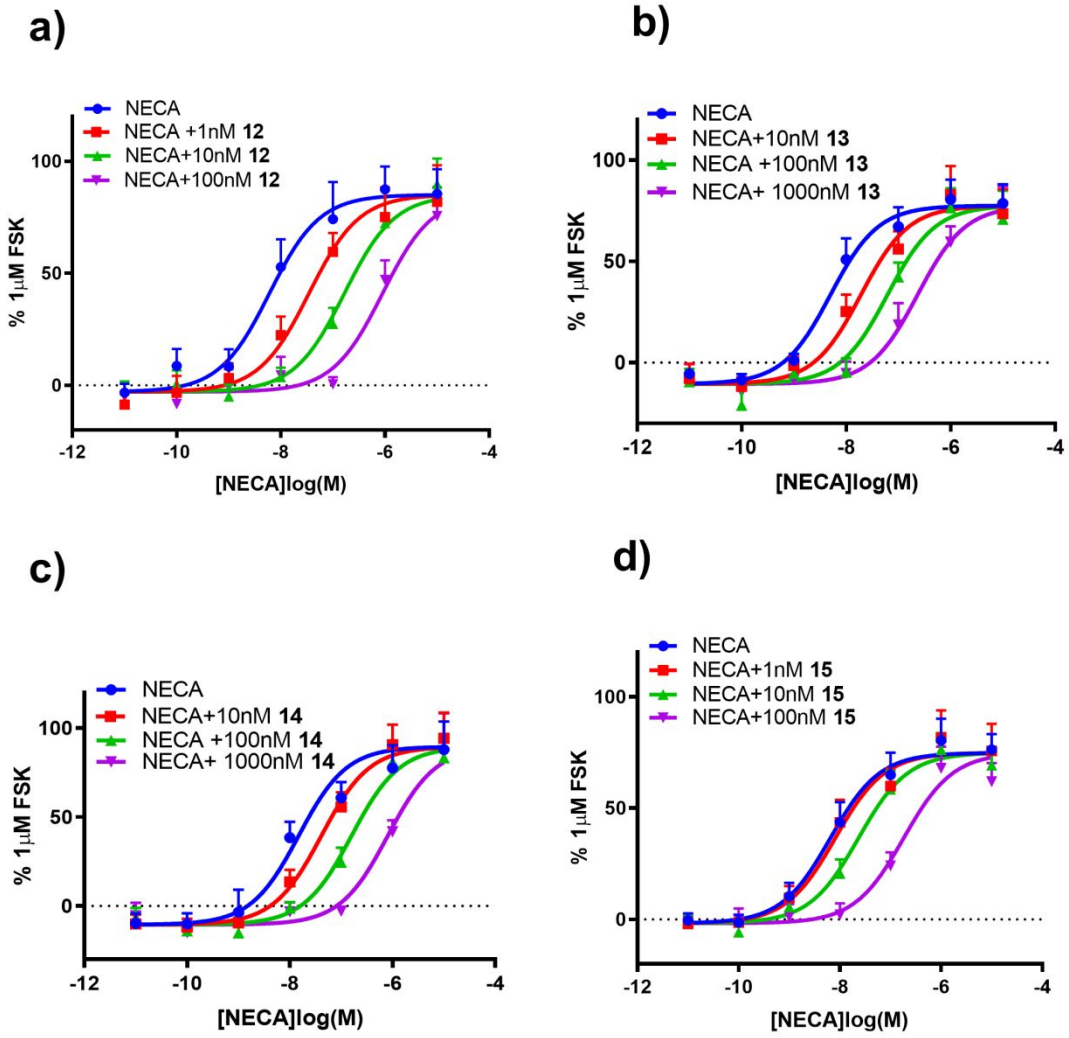

Figure 5. Inhibition of NECA-stimulated SPAP-secretion by the antagonists 12 (**a**), 13 (**b**), 14 (**c**) and 15 (**d**). CHO CRE-SPAP cells expressing the human A_{2A} receptor were stimulated with a concentration range of the agonist NECA in the absence and presence of the fluorescent antagonist of interest (1 nM, 10 nM, 100 nM for **12** and **15**; 10 nM, 100 nM, 1000 nM for **13** and **14).** Data have been expressed as a percentage of the SPAP production in response to serum-free media (0%) and to 1μM forskolin (FSK, 100%). The data shown represent the combined mean ± SEM of *n*=7 (**a**), *n*=6 (**b** and **d**) and *n*=5 (**c**) experiments, where each experiment was performed in triplicate.

The fluorescent ligands largely retained their functional antagonism as compared to the parent compound preladenant. Moreover, when comparing fluorescent ligands bearing a short linker (see Scheme 1) no significant difference in the measured functional affinity was observed ($p > 0.05$, comparing compounds **13** and **15**, unpaired t-test). Conversely, when comparing fluorescent ligands containing a longer linker the BODIPY 630/650 conferred 20-fold increase in affinity to the congener ($p < 0.05$, comparing compounds **12** and **14**, unpaired t-test). In this pharmacological assessment, compound **12** was the most potent of the series ($pA_2 = 9.31 \pm 0.38$, Figure 5A and Table 2). Interestingly, the affinity values measured *via* the NanoBRET saturation ligand binding assay (Table 1) were significantly lower compared to the affinity values obtained in CRE-SPAP gene-reporter assay (Table 2). The discrepancy in the affinity values is most likely due to the different host cell type and species (hamster versus human) employed in the two assays (CHO cells for CRE-SPAP and HEK293G cells for NanoBRET), the assay configuration (e.g. the influence of the furimazine substrate for NanoLuc) as well as the influence of the tag used in the NanoBRET experiments (transiently expressed NanoLuc-hA_{2A}AR for NanoBRET and stably expressed wild-type hA_{2A}AR for CRE-SPAP).[51] However, it is important to note that a small reduction in binding affinity of the fluorescent probe is not necessarily detrimental as long as the probe binds to the targeted receptor with sufficient specificity.[52]

Measuring the binding kinetics of a drug candidate is becoming extremely relevant considering the emerging concept that the rates at which a drug binds to its molecular target (k_{on}) and dissociates from it (k_{off}) may be considered more valuable parameters for predicting the effectiveness of a drug candidate in vivo.[53,54] In this regard, the BODIPY630/650-X-labelled analogue **12** was selected to be screened for its kinetic profile through a time-resolved fluorescence energy transfer (TR-FRET)[55–58] assay in membrane preparations from SNAP-

tagged-hA_{2A}AR-HEK293 cells (Figure 6). TR-FRET is a methodology which exploits proteins labeled with lanthanides (e.g. terbium) as donor fluorophores. Lanthanides display a long emission lifetime which allows for a time delay of the measurements between the excitation and the fluorescence of the acceptor fluorophore. This increases the sensitivity of the assay due to a reduction of the short-lived background fluorescence.[52,55,58] The TR-FRET technology allowed us to monitor the binding kinetics of **12** by measuring the observed association constant (K_{obs}) at four different concentrations of fluorescent ligand over a period of 1 h. The specific FRET signal was obtained by subtracting the non-specific signal (determined in the presence of 10 μM ZM241385) from the total signal at each time point. The kinetic parameters k_{on} = 2.4 ± 0.3 x 10^6 M^{-1} min^{-1}, k_{off} = 0.029 ± 0.004 min^{-1}, pK_D = 7.91 ± 0.06 and the residence time (1/ k_{off}) Tr = 35.36 ± 4.11 min, *n* = 5 were then calculated by globally fitting the resulting FRET data. This study revealed that fluorescent conjugate **12** has a relatively rapid on-rate but once bound dissociates slowly. In addition, from the 60 min time point we were also able to plot an equilibrium saturation curve of **12** and directly measure the equilibrium dissociation constant (K_D = 15.47 ± 1.92 nM, Figure S2) which was comparable to the value obtained from the kinetic analysis fit.

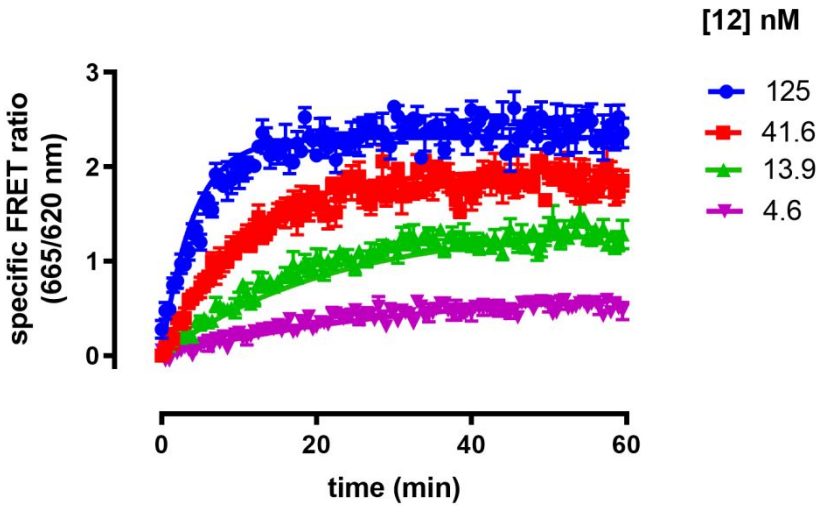

Figure 6. TR-FRET association kinetic curve of specific **12** binding to terbium-labelled SNAP-tagged-hA_{2A}AR-HEK293 cell membranes at 37°C. Cell membranes were treated with the indicated concentration of fluorescent ligand and the FRET signal was monitored every 30 s for 1 h. Non-specific binding was determined in the presence of 10 μM ZM241385. The graph presented is a representative of n = 5 experiments performed in triplicate.

Interestingly we found that the binding affinity pK_D of **12** measured in this kinetic study (7.91 ± 0.06) in HEK293G cell membranes was similar to the pK_D (7.39 ± 0.05) measured in the same cells in NanoBRET experiments. These data suggest that the large difference in observed binding affinity for **12** between NanoBRET experiments in HEK293G cells and CRE-SPAP functional experiments in CHO-K1 cells is largely due to the host cellular environment. Having established that the novel fluorescent probes retain functional activity and binding affinity at the hA_{2A}AR we next evaluated their utility for confocal microscope imaging studies. Ideally, the novel fluorescent ligands should bind specifically to the A_{2A}AR receptors on the cell surface and show both low levels of nonspecific binding and diffusion into the cell cytosol. From the BODIPY-labelled probes, we selected compounds **12** (red-emitting) and **15** (green-emitting) (Scheme 1) and determined whether the selected compounds were suitable for visualization of receptors in

live cells. To this end confocal microscopy was conducted on HEK293 cells expressing the SNAP-tagged $hA_{2A}AR$ (Figure 7). The images captured with the confocal microscope revealed that both compounds **12** and **15** bound specifically to the SNAP-tagged $hA_{2A}AR$ shown by the high level of fluorescence localized at the cell membrane. Pre-incubation with 1 μM of unlabeled antagonist ZM241385 produced a significant reduction of the fluorescence intensity and very little intracellular fluorescence was observed. This demonstrated that binding of both compounds was specific at the SNAP-tagged $hA_{2A}AR$ as it was surmounted by high concentration of unlabeled $hA_{2A}AR$ antagonist.

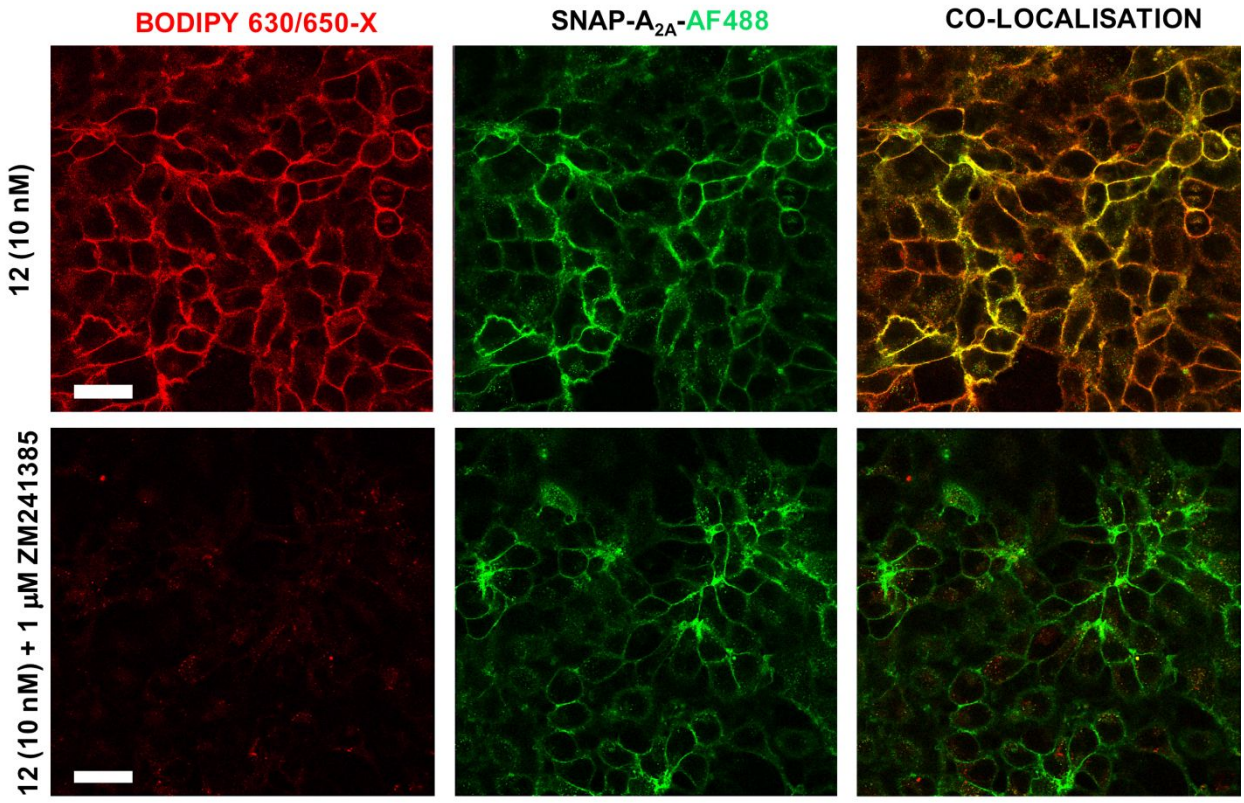

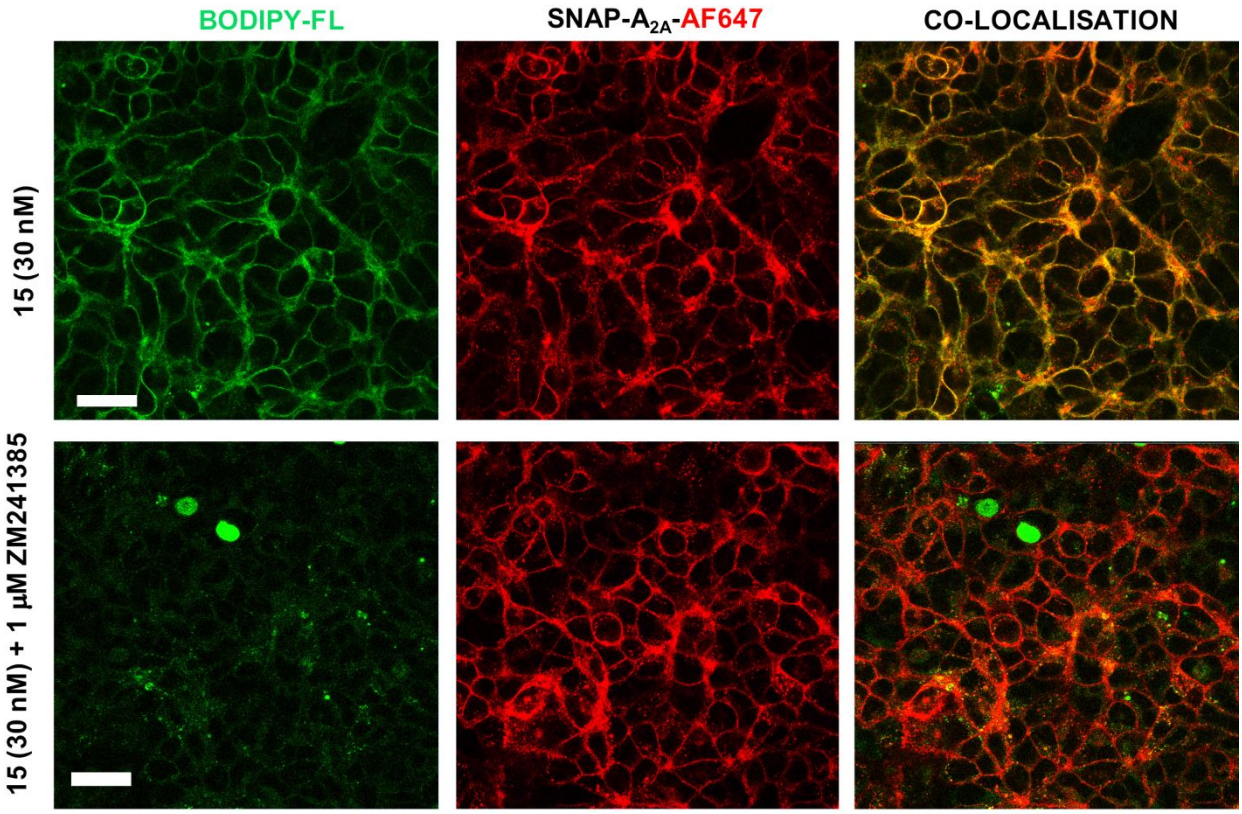

Figure 7. Live cell confocal imaging of **12** (10 nM) and **15** (30 nM) binding to SNAP-tagged *h*A_{2A}AR HEK293 cells in the absence or presence of 1 μM of unlabelled antagonist ZM241385. Cells were incubated at 37°C with BG-AlexaFluor488 when imaging red-shifted ligands (**12**) or BG-AlexaFluor647 to label the SNAP-tag on the N-terminus of the receptor when imaging green-shifted ligands (**15**) (middle frames). Images are representative of images captured in three separate experiments (scale bar 20 μm).

We also investigated whether the water-soluble hA_{2A}AR fluorescent ligands were able to allow receptor visualization through confocal imaging. The results revealed that probes **16** and **17** bind to the SNAP-tagged *h*A_{2A}AR as demonstrated by the high degree of fluorescence observed at the cell membranes (Figure 8). Most importantly, the binding of the two ligands to the A_{2A}AR was highly specific as pre-incubation with 1 μM ZM241385 completely inhibited the binding of each fluorescent ligand. Very little non-specific binding was detected and rewardingly, no measurable uptake of these ligands into in the cytosol could be seen.

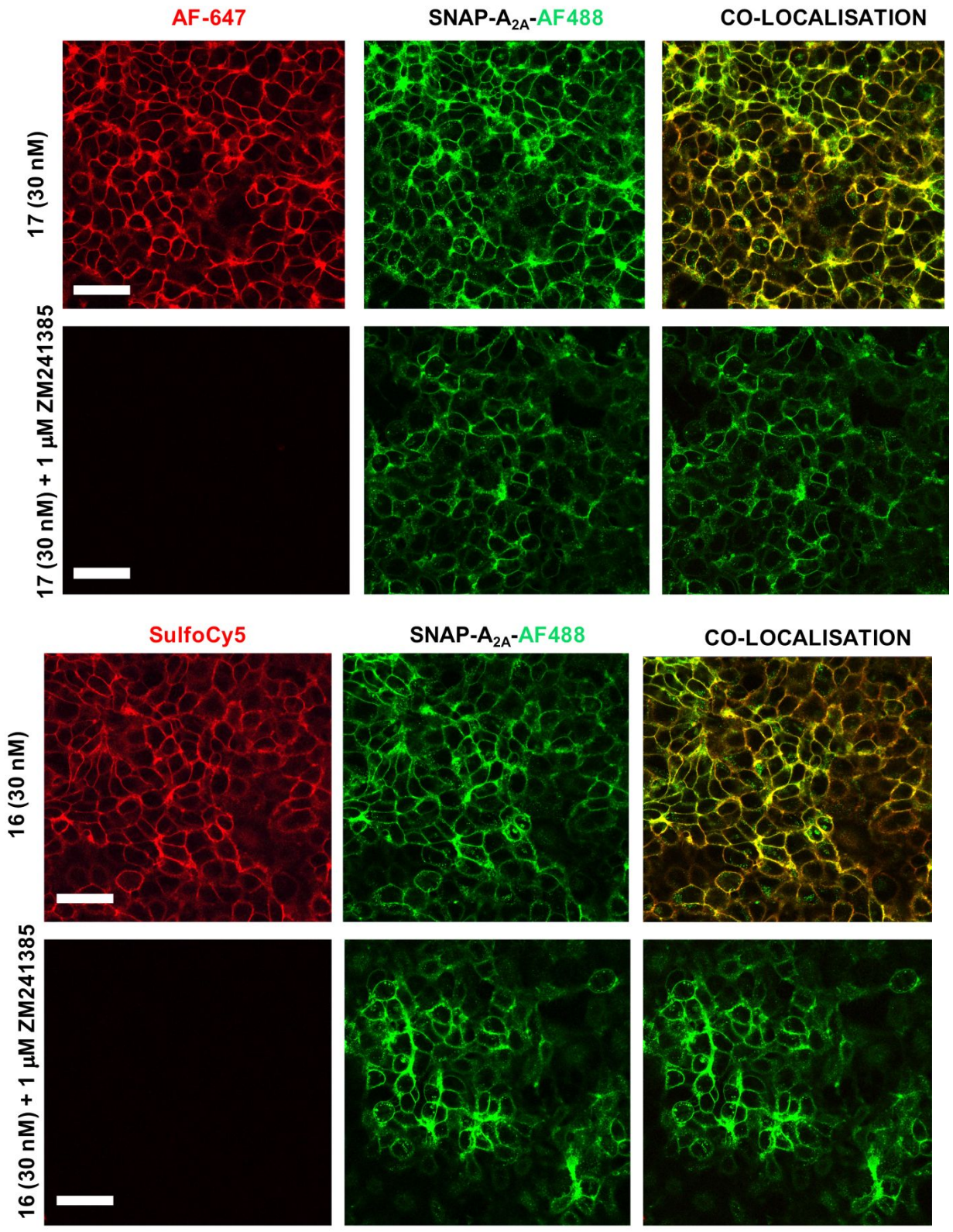
AF-647
SNAP-A2A-AF488
CO-LOCALISATION
17 (30 nM)
17 (30 nM) + 1 µM ZM241385
SulfoCy5
SNAP-A2A-AF488
CO-LOCALISATION
16 (30 nM)
16 (30 nM) + 1 µM ZM241385

Figure 8. Live cell confocal imaging of **16** (30 nM) and **17 (**30 nM) binding to SNAP-tagged $hA_{2A}AR$ expressed in HEK293 cells. Cells were incubated 30 min at 37°C with BG-AlexaFluor488 prior incubation in the absence or presence of 1 μM ZM241385. Subsequently, cells were incubated with 30 nM fluorescent ligand for 30 min at 37°C prior to imaging. The images generated are from one single experiment and are representative of three different experiments. The images were all captured using the same settings for laser power and detector gain. Scale bars are 50 μm.

Compound **17** was selected for further studies. In particular, the utility of AlexaFluor647-bearing probe **17** in measuring the binding affinities of unlabelled $hA_{2A}AR$ antagonists was investigated using the NanoBRET competition ligand binding assay. HEK293 cells transiently expressing the NanoLuc-$hA_{2A}AR$ were incubated with **17** (50 nM) and increasing concentrations of the $hA_{2A}AR$ antagonists ZM241385, SCH58261, SCH442416 and MRS1334 a selective adenosine A_3AR antagonist which was used as negative control. A concentration dependent decrease of the BRET signal was observed for the $A_{2A}AR$ selective compounds, allowing the binding affinities of the unlabeled antagonists to be measured (Figure 9 and Table 3). The values obtained through fluorescent binding assays were comparable to the reported literature values (R^2 = 0.97, Figure S1) measured in radioligand binding experiments.[4,59] No concentration-dependent decrease of the BRET signal was observed in the presence of the selective A_3AR antagonist MRS1224 confirming the specificity of the binding of the probe **17** to the $A_{2A}AR$.

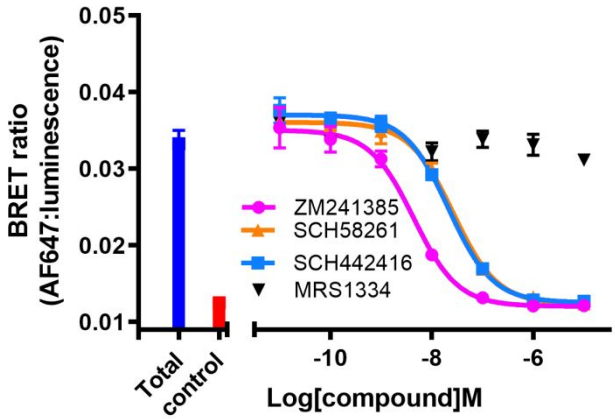

Figure 9. Displacement of **17** (50 nM) by unlabeled $hA_{2A}AR$ antagonists ZM241385, SCH58261, SCH442416 and hA_3AR antagonist MRS1334 in HEK293G cells transiently expressing the Nanoluc-$hA_{2A}AR$. Blue and red bars represent the total BRET signal of **17** in absence or presence of ZM241385 (10 μM) respectively. The decrease in BRET ratio was monitored as a function of increasing concentration of unlabeled antagonist. Each data point represents mean value ± SEM of triplicate determinations in a single representative experiment of $n = 4$ experiments.

Table 3. Binding affinities (pK_i) of target $hA_{2A}AR$ antagonists calculated from Cheng-Prusoff analysis of the data displayed in Figure 9.

Compound	**pK_i** (BRET binding assay)	**pK_i** (literature). [a]
ZM241385	8.84 ± 0.09	8.80 [b]
SCH58261	7.92 ± 0.10	8.30 [c]
SCH442416	7.90 ± 0.10	8.38 [d]

[a] Reported binding affinities of target $hA_{2A}AR$ antagonists. [b, c] Values determined in radioligand binding experiments in CHO-hA_{2A} and HEK293-hA_{2A} cells using [H^3] SCH58261.[59,60] [d] Values determined in HEK293-hA_{2A} using the radiolabelled agonist [^{3}H] CGS

21680.[30] The data measured through NanoBRET competition ligand binding assay are means ± SEM of $n = 4$ experiments performed in triplicate.

CONCLUSION

In the present study, we have reported the successful design, development and pharmacological evaluation of a novel series of $hA_{2A}AR$ fluorescent antagonists, encompassing BODIPY-bearing probes and water soluble Cy5-labelled and AF647-labelled probes, based on the high affinity and selective preladenant scaffold. In particular, derivatization of the amino functionalized congener **11** with two families of fluorescent tags led to six $hA_{2A}AR$ fluorescent antagonists with retained affinity and, most importantly, selectivity at the $A_{2A}AR$ subtype. Both families of compounds allowed visualization of $A_{2A}ARs$ expressed in live cells as demonstrated by the high fluorescence intensity at the cell membranes. The binding of these fluorescent ligands could be surmounted by a high concentration of ZM241385 confirming that the binding of the probes was specific. Very little non-specific binding was observed for the water-soluble fluorescent antagonists (Figure 8). Within the water-soluble family of probes, fluorescent conjugate **17** was selected to successfully monitor ligand binding of reported $hA_{2A}AR$ antagonists (Figure 9 and Table 3).

The novel $hA_{2A}AR$ fluorescent ligands developed can be broadly applied in a series of fluorescence-based techniques to study the signaling and dynamics of the adenosine $A_{2A}AR$ receptors in their native cellular environment spanning from in vitro to in vivo applications. Most importantly we believe that these ligands in combination with the NanoBRET approach and bioimaging studies can help to shed light on the complexity of the $A_{2A}AR$ signaling in different biological elements and during disease progression. This ultimately should provide useful

insights concerning specific A_{2A}AR-engagement in several disease phenotypes, including cancer.[13,61,62]

EXPERIMENTAL SECTION

Chemistry: Materials and Methods

Chemicals and solvents of analytical and HPLC grade were purchased from commercial suppliers and used without further purification. BODIPY630/650-X-SE, BODIPY-FL-X-SE, and BODIPY-FL-SE were purchased from Molecular Probes (Thermo Fisher Scientific). AlexaFluor647 NHS ester was purchased from Thermo Fischer Scientific and Sulfo-Cyanine5 NHS ester from Lumiprobe. All reactions were carried out at ambient temperature unless otherwise stated. Reactions were monitored by thin-layer chromatography on commercially available silica pre-coated aluminium-backed plates (Merck Kieselgel 60 F^{254}). Visualisation was under UV light (254 nm and 366 nm), followed by staining with ninhydrin or $KMnO_4$ dips. Flash column chromatography was performed using silica gel 60, 230-400 mesh particle size (Sigma Aldrich). NMR spectra were recorded on a Bruker-AV 400. ^{1}H NMR spectra were recorded at 400.13 MHz and ^{13}C NMR spectra at 101.62 MHz. All ^{13}C NMR are ^{1}H broadband decoupled. Solvents used for NMR analysis (reference peaks listed) were $CDCl_3$ supplied by Cambridge Isotope Laboratories Inc., (δH = 7.26 ppm, δC = 77.16) Chemical shifts (δ) are recorded in parts per million (ppm) and coupling constants are recorded in Hz. The following abbreviations are used to described signal shapes and multiplicities; singlet (s), doublet (d), triplet (t), quadruplet (q), broad (br), dd (doublet of doublets), ddd (double doublet of doublets), dtd (double triplet of doublets) and multiplet (m). Processing of the NMR data was carried out using the NMR software Topspin. LC-MS spectra were recorded on a Shimadzu UFLCXR system coupled to an

Applied Biosystems API2000 and visualised at 254 nm (channel 1) and 220 nm (channel 2). LC-MS was carried out using a Phenomenex Gemini-NX C18 110A, column (50 mm × 2 mm x 3 μm) at a flow rate 0.5 mL/min over a 5 min period (Method A). All high resolution mass spectra (HRMS) were recorded on a Bruker microTOF mass spectrometer using MS electrospray ionization operating in positive ion mode. RP-HPLC was performed on a Waters 515 LC system and monitored using a Waters 996 photodiode array detector at wavelengths between 190 and 800 nm. Spectra were analysed using Millenium 32 software. Semi-preparative HPLC was performed using YMC-Pack C8 column (150 mm × 10 mm × 5 μm) at a flow rate of 5.0 mL/min using a gradient method of 20-70% B over 21 minutes (Solvent A = 0.01% formic acid in H_2O, solvent B = 0.01% formic acid in CH_3CN (Method B)). Analytical RP-HPLC was performed using a YMC-Pack C8 column (150 mm × 4.6 mm × 5 μm) and a Phenomenex Gemini NX-C18 column (250 mm × 4.6 mm × 5 μm) at a flow rate of 1.0 mL/min. Final products were one single peak and >98% pure. The retention time of the final product is reported using a gradient method of 10-90% solvent B in solvent A over 30 min. (Solvent A = 0.01% formic acid in H_2O, solvent B = 0.01% formic acid in CH_3CN (Method C)).

General Procedure 1: Synthesis of Fluorescent Conjugates. The amine congener (as the di-HCl salt) was dissolved in DMF (0.5 mL), treated with DIPEA (0.6 μL 3.7 mmol, 4 eq.) and then reacted with BODIPY630/650–X-NHS (0.5 mg, 1 eq.), BODIPY-FL-X-NHS (1 eq., 0.5 mg), BODIPY-FL-NHS (1 eq., 0.5 mg), Sulfo-Cyanine5-NHS ester (0.8 mg, 1 eq.), AlexaFluor647-NHS (0.8 mg, 1 eq.) and HATU (1.7 mg, 1 eq.) prior reacting with BODIPY630/650-carboxylic acid (2 mg). The resulting solution was stirred at RT under the exclusion of light for 1-5 h. Upon completion of the reaction monitored by LC-MS, the solution was concentrated to dryness and

the residue was dissolved in 1:1 CH_3CN/H_2O. Purification by reverse phase-HPLC, followed by lyophilization, afforded the pure fluorescent conjugate.

7-(2-Chloroethyl)-2-(furan-2-yl)-7*H*-pyrazolo[4,3-*e*][1,2,4]triazolo[1,5-*c*]pyrimidin-5-amine *(4)*. 2-amino-4,6-dichloropyrimidine-5-carbaldehyde (0.5 g, 2.6 mmol, 1 eq.) was dissolved in anhydrous THF (20 mL). To the resulting mixture was added Et_3N (0.26 g, 2.86 mmol, 1.1 eq.) followed by 2- furoic hydrazide (0.36 g, 2.86 mmol, 1.1 eq.). The above mixture was heated to 70°C for 3 h. The mixture was then evaporated *in vacuo* to give intermediate **2** as yellow solid which was used for the next reaction without further purification. LC-MS *m/z* calc. for $C_{10}H_9ClN_5O_3$ $[MH]^+$ 282.04; found 282.10, t_R= 2.09min (Method A). To a solution of **2 (**1 eq.) in CH_3CN/water (10:2.5 mL) was added 2-hydrazinoethanol (0.35 mL, 5.2 mmol, 2 eq.). The mixture was heated to reflux for 2.5 h. The solution was allowed to cool at RT. 0.1M HCl (5 mL) was added to the reaction mixture. Afterwards, the solution was evaporated *in vacuo* to 5mL and left overnight for a solid to appear. Water (10 mL) was added and the solid was collected by filtration. The solid was further washed with CH_3CN and Et_2O. The solid was dissolved in MeOH and the solution was evaporated azeotropically with toluene to give the desired compound **3** which was used for the next step without any further purification. LC-MS *m/z* calc. for $C_{12}H_{14}N_7O_3$ $[MH]^+$ 304.12; found 304.10, t_R = 0.61 min (Method A). Intermediate **3** (0.550 g, 1.8 mmol, 1 eq) was dissolved in $POCl_3$ (4 mL). To the resulting mixture was added $ZnBr_2$ (0.1 g). The mixture was heated to 80°C for 5 h. Then, $POCl_3$ was evaporated, water (ice) added and the resulting aqueous solution was extracted with EtOAc. Organic layers were collected, dried over Na_2SO_4 anhydrous, filtered and evaporated to dryness. Purification by flash column chromatography on silica gel using 2:1 EtOAc/Pet. Spirits gave a mixture of intermediates **4a** and **4b** as a pale yellow solid (0.11 g, yield 11%). LC-MS *m/z* calc. for $C_{12}H_{11}ClN_7O$ $[MH]^+$

304.07; found 304.10; calc. for $C_{12}H_{10}BrN_7O$ $[MH]^+$ 348.02; found 348.10, t_R = 2.50 min (Method A). ^1H NMR (DMSO-d_6) δ 8.23 (s, *J* = 1.0 Hz, 1H), 8.14 (brs, 2H), 7.95 (d, *J* = 1.8 Hz, 1H), 7.24 (d, *J* = 3.3 Hz, 1H), 6.74 (dd, *J* = 3.4, 1.8 Hz, 1H), 4.66 (t, *J* = 6.2 Hz, 1H), 4.60 (t, *J* = 5.9 Hz, 2H), 4.09 (t, *J* = 5.9 Hz, 2H), 3.94 (t, *J* = 6.2 Hz, 1H).

2-(2-((*tert*-Butoxycarbonyl)amino)ethoxy)ethyl 4-methylbenzenesulfonate ***(6)***. *tert*-Butyl (2-(2-hydroxyethoxy) ethyl) carbamate (1 g, 4.87 mmol, 1 eq.) was dissolved in DCM (20 mL). To the resulting mixture were added DIPEA (2.5 mL, 3 eq.), DMAP (5%mol) and TsCl (1.85 g, 9.74 mmol, 1.3 eq.). The mixture was stirred at RT overnight. The solution was concentrated under reduced pressure to a volume of 5mL. Purification by flash column chromatography on silica gel using a gradient of 0→4% MeOH/DCM gave the desired product, (1.5 g, yield 86%) LC-MS *m/z* calc. for $C_{16}H_{26}NO_6S$ $[MH]^+$360.15; found 360.10; t_R = 2.51min (Method A). ^1H NMR ($CDCl_3$) δ 7.80 (d, *J* = 8.0 Hz, 2H), 7.35 (d, *J* = 7.96 Hz, 2H), 4.80 (brs, 1H), 4.16 (t, *J* = 4.1 Hz, 2H), 3.63 (t, *J* = 4.3 Hz, 2H), 3.45 (t, *J* = 4.4 Hz, 2H), 3.24 (q, *J* = 5.4 Hz, 2H), 2.45 (s, 3H), 1.45 (s, 9H). ^{13}C NMR ($CDCl_3$) δ 155.9, 145.0, 133.1, 129.9, 128.1, 79.4, 70.4, 69.2, 68.4, 40.3, 28.5, 21.7.

Benzyl 4-(4-hydroxyphenyl)piperazine-1-carboxylate ***(8)***. Benzyl chloroformate (0.793 mL, 5.6 mmol, 1eq.) was added to a stirred suspension of 4-(piperazin-1-yl) phenol and K_2CO_3 in DMF (8 mL). Water was then added and the aqueous layer was extracted with EtOAc. The organic layer was further washed with water (x3), dried over anhydrous Na_2SO_4, filtered and evaporated to dryness. Purification by flash column chromatography on silica using 40% EtOAc/Pet. ether gave the desired product (1.2 g, yield 66%) LC-MS *m/z* calc. for $C_{18}H_{21}N_2O_3$ $[MH]^+$ 313.15; found 313.10; t_R = 2.51 min (Method A). ^1H NMR ($CDCl_3$) δ 7.39 – 7.31 (m, 5H), 6.85 (d, *J* = 8.4 Hz 2H), 6.77 (d, *J* = 7.6 Hz, 2H), 5.17 (brs, 1H), 5.00 (s, 2H), 3.66 (t, *J* =

4.63 Hz 4H), 3.01 (m, 4H). ^{13}C NMR ($CDCl_3$) δ 155.1, 136.4, 128.4, 127.9, 127.8, 119.1, 115.8, 67.1, 50.9, 43.7(two quaternary carbons in the phenol not observed).

Benzyl 4-(4-(2-(2-((*tert*-butoxycarbonyl)amino)ethoxy)ethoxy)phenyl)piperazine-1-carboxylate (9i) Compound **8** (0.36 g, 1.16 mmol) was dissolved in CH_3CN (10 mL). K_2CO_3 (0.5 g) was subsequently added to the reaction mixture followed by compound **6** (0.416 g, 1.16 mmol, 1eq). The resulting mixture was heated to 100°C and held at this temperature for 6 h. The reaction was allowed to cool, Et_2O was added and the mixture was washed with 1M NaOH (x3). The organic layer was collected and evaporated to dryness. Purification by flash column chromatography on silica using 60% EtOAc/Pet. ether gave the final product as an off-white solid (0.2 g, yield 40%) LC-MS *m/z* calc. for $C_{27}H_{38}N_3O_6$ $[MH]^+$ 500.28; found 500.10; t_R = 3.02 min (Method A). ^{1}H NMR ($CDCl_3$) δ 7.40 – 7.32 (m, 5H), 6.88 (s, 4H), 5.16 (s, 2H), 4.98 (brs, 1H), 4.07 (t, *J* = 4.3Hz, 2H), 3.79 (t, *J* = 4.5Hz, 2H), 3.66 (t, *J* = 4.8 Hz, 4H), 3.60 (t, *J* = 4.8Hz, 2H), 3.34 (q, *J* = 4.6 Hz, 2H), 3.07 – 2.97 (m, 4H), 1.44 (s, 9H). ^{13}C NMR ($CDCl_3$) δ 155.4, 150.1, 136.4, 128.4, 127.9, 127.79, 115.3, 70.2, 69.4, 67.6, 67.1, 50.7, 43.7, 40.2, 28.2.

***tert*-Butyl (2-(2-(4-(piperazin-1-yl)phenoxy)ethoxy)ethyl)carbamate (9ii)** Compound **9i** (0.2 g, 1eq) was dissolved in EtOH(4 mL) and the resulting mixture was stirred at RT under a nitrogen atmosphere. Pd/C 11% w/w was added to the reaction mixture and the flask was evacuated and replaced with a H_2 atmosphere. The reaction was stirred at RT for 3h. The Completion of the reaction was confirmed by TLC. The mixture was then filtered through Celite™ and the pad was washed with EtOH (40 mL) and DCM (40 mL x 3). The filtrate was collected and concentrated under reduced pressure to give the pure product as an off-white solid (0.12 g, yield 82%). LC-MS *m/z* calc. for $C_{19}H_{32}N_3O_4$ $[MH]^+$ 366.24; found 366.10; t_R = 2.12 min (Method A). ^{1}H NMR ($CDCl_3$) δ 6.92 – 6.84 (m, 4H), 5.00 (brs, 1H), 4.07 (t, *J* = 4.4 Hz,

2H), 3.79 (t, *J* = 4.4 Hz, 2H), 3.60 (t, *J* = 4.4 Hz, 2H), 3.47 (s, 1H), 3.33 (q, *J* = 4.8 Hz, 2H), 3.05 (s, 7H), 1.44 (s, 9H). ^{13}C NMR ($CDCl_3$) δ 156.1, 153.1, 146.5, 118.4, 115.5, 79.37, 70.5, 69.7, 67.9, 51.7, 46.2, 40.5, 28.5.

tert*-Butyl (2-(2-(4-(4-(2-(5-amino-2-(furan-2-yl)-7*H*-pyrazolo[4,3-*e*][1,2,4]triazolo[1,5-*c*]pyrimidin-7-yl)ethyl)piperazin-1-yl)phenoxy)ethoxy)ethyl)carbamate** ***(10) *tert*-Butyl (2-(2-(4-(piperazin-1-yl)phenoxy)ethoxy)ethyl)carbamate (30 mg, 0.9 μmol, 1eq) and **4** (40 mg, $0.11x10^{-5}$ mol, 1eq) were dissolved in DMF (0.5 mL) prior to the addition of DIPEA (4 eq., 0.4 mL). The resulting mixture was heated and held at 100°C overnight. Completion of the reaction was confirmed by TLC. The solution was further dissolved in EtOAc and washed with water (x3). The organic layer was collected and concentrated under reduced pressure. Purification by flash column chromatography on silica using DCM:MeOH (96:4) gave the pure compound as a pale yellow solid (12 mg, yield 19%). LC-MS *m/z* calc. for $C_{31}H_{41}N_{10}O_5$ $[MH]^+$ 633.33; found 633.10; t_R = 2.12 min (Method A). ^{1}H NMR ($CDCl_3$) δ 8.18 (s, 1H), 7.53 (d, *J* = 1.8 Hz, 1H), 7.21 (d, *J* = 3.4 Hz, 1H), 6.88 – 6.81 (m, 4H), 6.56 (dd, *J* = 3.5, 1.8 Hz, 1H), 6.45 (brs, 2H), 5.01 (brs, 1H), 4.53 (t, *J* = 6.42 Hz, 2H), 4.05 (t, *J* = 3.72 Hz, 2H), 3.78 (t, *J* = 4.2 Hz, 2H), 3.59 (t, *J* = 4.1 Hz, 2H), 3.33 (q, *J* = 5.1 Hz), 3.14 – 3.07 (m, 4H), 2.98 (t, *J* = 6.00 Hz, 2H), 2.78 – 2.69 (m, 4H), 1.43 (s, 9H). ^{13}C NMR ($CDCl_3$) δ 156.7, 156.1, 152.9, 149.3, 148.3, 145.9, 145.5, 145.5, 144.7, 132.3, 118.1, 115.5, 112.7, 112.1, 97.4, 79.4, 70.5, 69.7, 67.9, 57.0, 53.4, 50.4, 45.3, 40.5, 28.5.

7-(2-(4-(4-(2-(2-Aminoethoxy) ethoxy) phenyl) piperazin-1-yl) ethyl)-2-(furan-2-yl)-7*H*-pyrazolo[4,3-*e*][1,2,4]triazolo[1,5-*c*]pyrimidin-5-amine (***11***) Compound **10** (12 mg, 1 eq.) was dissolved in 4 M HCl in dioxane (1 mL). The completion of the reaction was confirmed by TLC and LC-MS after 30min.The solvent was removed under reduced pressure and the compound

was used in the next synthetic step without further purification. (10 mg, quantitative 100%) LC-MS *m/z* calc. for $C_{26}H_{33}N_{10}O_3$ $[MH]^+$ 533.27; found 533.10; t_R = 1.85 min (Method A).

(E)-*N*-(2-(2-(4-(4-(2-(5-Amino-2-(furan-2-yl)-7*H*-pyrazolo[4,3-*e*][1,2,4]triazolo[1,5-*c*]pyrimidin-7-yl)ethyl)piperazin-1-yl)phenoxy)ethoxy)ethyl)-6-(2-(4-(2-(5,5-difluoro-7-(thiophen-2-yl)-5*H*-5l^4,6l^4-dipyrrolo[1,2-*c*:2',1'-*f*][1,3,2]diazaborinin-3-yl)vinyl)phenoxy)acetamido)hexanamide (*12)*.** Following general procedure 1, amine congener **11** (0.5 mg, 1 eq.) was converted to the BODIPY630/650–X conjugate **12**. Purification by RP-HPLC (Method B) gave, after lyophilization, the title compound as a blue solid (1.1 mg 98%). Analytical RP-HPLC t_R =15.48 min (Method C), purity >98%. HRMS (ESI-TOF) calc. for $C_{55}H_{59}BF_2N_{13}O_6S$ $[M+H]^+$1078.4488; found 1078.4508 and 1100.4307 [M+Na].

(E)-*N*-(2-(2-(4-(4-(2-(5-Amino-2-(furan-2-yl)-7*H*-pyrazolo[4,3-*e*][1,2,4]triazolo[1,5-*c*]pyrimidin-7-yl)ethyl)piperazin-1-yl)phenoxy)ethoxy)ethyl)-2-(4-(2-(5,5-difluoro-7-(thiophen-2-yl)-5*H*-4l^4,5l^4-dipyrrolo[1,2-*c*:2',1'-*f*][1,3,2]diazaborinin-3-yl)vinyl)phenoxy)acetamide *(13).* Following general procedure 1, amine congener **11** (1 eq, 0.5 mg) was converted to the BODIPY630/650 conjugate **13**. Purification by RP-HPLC (Method B) gave, after lyophilization, the title compound as a blue solid (1 mg, yield 56%) Analytical RP-HPLC t_R =15.30 min (Method C), purity >99%. HRMS (TOF ES^+) calc. for $C_{49}H_{48}BF_2N_{12}O_5S$, $[M+H]^+$ 965.3574; found 965.3593

***N*-(2-(2-(4-(4-(2-(5-Amino-2-(furan-2-yl)-7*H*-pyrazolo[4,3-*e*][1,2,4]triazolo[1,5-*c*]pyrimidin-7-yl)ethyl)piperazin-1-yl)phenoxy)ethoxy)ethyl)-6-(3-(5,5-difluoro-7,9-dimethyl-5*H*-4l^4,5l^4-dipyrrolo[1,2-*c*:2',1'-*f*][1,3,2]diazaborinin-3-yl)propanamido)hexanamide** *(14)*. Following general procedure 1, amine congener **11** (1 eq., 0.5 mg) was converted to the BODIPY-FL–X conjugate **14**. Purification by RP-HPLC (Method B) gave, after lyophilization, the title compound

as an orange solid, (1.2 mg, yield 70%). Analytical RP-HPLC t_R =13.04 min (Method C) purity >99%. HRMS (TOF ES$^+$) calc. for $C_{46}H_{57}BF_2N_{13}O_5$, $[MH]^+$ 920.4588, found 920.4660.

N*-(2-(2-(4-(4-(2-(5-Amino-2-(furan-2-yl)-7*H*-pyrazolo[4,3-*e*][1,2,4]triazolo[1,5-*c*]pyrimidin-7-yl)ethyl)piperazin-1-yl)phenoxy)ethoxy)ethyl)-3-(5,5-difluoro-7,9-dimethyl-5*H*-4*l*^{4},5*l*^{4}-dipyrrolo[1,2-*c*:2',1'-*f*][1,3,2]diazaborinin-3-yl)propanamide** ***(15). Following general procedure 1, amine congener **11** (1 eq., 0.5 mg) was converted to the BODIPY–FL conjugate **15.** Purification by RP-HPLC (Method B) gave, after lyophilization, the title compound as an orange solid (0.7 mg, yield 100%). Analytical RP-HPLC t_R =13.13 min (Method C), purity >99%. HRMS (TOF ES$^+$) calc. for $C_{40}H_{46}BF_2N_{12}O_4$, $[MH]^+$ 807.3821, found 807.3820 and calc. for $C_{40}H_{45}BF_2N_{12}O_4Na$ [M+Na] 829.3640, found 829.3627.

1-(6-((2-(2-(4-(4-(2-(5-Amino-2-(furan-2-yl)-7*H*-pyrazolo[4,3-*e*][1,2,4]triazolo[1,5-*c*]pyrimidin-7-yl)ethyl)piperazin-1-yl)phenoxy)ethoxy)ethyl)amino)-6-oxohexyl)-3,3-dimethyl-2-((1*E*,3*E*)-5-((*E*)-1,3,3-trimethyl-5-sulfoindolin-2-ylidene)penta-1,3-dien-1-yl)-3*H*-indol-1-ium-5-sulfonate ***(16)***. Following general procedure 1, amine congener **11** (1 eq, 0.5 mg) was converted to Sulfo-Cyanine-5 conjugate **16**. Purification by RP-HPLC (Method B) gave, after lyophilization, the title compound as bright blue solid (1.9 mg, yield quantitative 100%) pure. Analytical RP-HPLC t_R=12.41 min (Method C) purity >99%. HRMS (TOF ES$^-$) $C_{58}H_{68}N_{12}O_{10}S_2$, $[MH]^-$ calculated 1155.4550, found 1155.4547

3-(6-((2-(2-(4-(4-(2-(5-Amino-2-(furan-2-yl)-7*H*-pyrazolo[4,3-*e*][1,2,4]triazolo[1,5-*c*]pyrimidin-7-yl)ethyl)piperazin-1-yl)phenoxy)ethoxy)ethyl)amino)-6-oxohexyl)-2-((1*E*,3*E*)-5-((*E*)-3,3-dimethyl-5-sulfo-1-(3-sulfopropyl)indolin-2-ylidene)penta-1,3-dien-1-yl)-3-methyl-5-sulfo-1-(3-sulfopropyl)-3*H*-indol-1-ium ***(17)***. Following general procedure 1,

amine congener **11** (1 eq., 0.5 mg) was converted to the AlexaFluor647 conjugate **17**. Purification by RP-HPLC (Method B) gave the title compound as bright blue solid (1.8 mg quantitative 100%). Analytical RP-HPLC t_R =10.58 min (Method C) purity >99%. HRMS (TOF ES$^-$) calc. for $C_{62}H_{76}N_{12}O_{16}S_4$, [MH]- 1372.4355; found 1372.4391 [M-2]$^-$ calculated 685.2120 found 685.2122.

Molecular Modelling of Preladenant

Docking of preladenant to the high resolution hA_{2A}AR crystal structure was performed using Schrodinger software suite (release 2018-3). The 1.8 angstrom resolution hA_{2A}AR crystal structure was imported from the Protein Data Bank (PDB = 4EIY) and was prepared with the Protein Preparation Wizard program. This involved removal of water molecules, co-crystalized head groups, with the exclusion of the co-crystalized ligand ZM241385, and the addition of hydrogen atoms. The H-bonding network was optimized using PROPKA at pH = 7 and ultimately the protein structure was energy minimized by using OPLS3 force field. The docking site was defined with Glide Grid generation by using the coordinates of the co-crystallized ligand ZM241385. Preladenant was prepared for docking using LigPrep program. Molecular docking of preladenant was performed using Glide with XP (extra precision) mode and flexible ligand sampling without applying any restriction. Ten poses were generated and the highest glide scoring pose was selected and modelled with PyMOL (version 2.2.0) to include key binding residues and distances measurements.

Pharmacology: Material and Methods

Cell culture reagent were purchased from Sigma Chemicals (Pool, Dorset, UK) except Fetal Calf Serum (FCS) which was provided by PAA Laboratories (Teddington, Middlesex, UK). G418

and Optimem were obtained from Life Technologies (Paisley, UK). SNAP-Lumi4-Tb was obtained by Cisbio Bioassays (Bagnols-sur-Cèze, France). All plates were obtained from Corning Costar (Corning Incorporated, Corning, NY, USA) unless otherwise stated. FuGENE® transfection reagent and furimazine were purchased from Promega (Southampton, UK). ZM243185 was purchased from Tocris Bioscience (Bristol, UK). All other chemical and reagents were purchased from Sigma-Aldrich (Gillingham, UK)

Cell culture A CHO cell line stably expressing cAMP response element-secreted placental alkaline phosphatase (CRE-SPAP) reporter gene and the human A_2AR were generated as previously described[55]. CHO A_{2A} CRE-SPAP cell lines were cultured in Dulbecco's modified Eagle's medium (DMEM-F12) nutrient mix supported by 10% heat-inactivated FCS and 2mM L-glutamine. HEK293 cells stably expressing Nluc-A_1 and Nluc-A_3 were as described previously[63]. To generate cells stably expressing the Nluc-A_{2B} HEK293 cells were stably transfected with pcDNA-Nluc-A_{2B} using FUGENE® reagent, following the manufacturer's instructions, using 2:1 reagent:DNA ratio. Transfected cells were selected using 1 μg/mL G418. Cells were cultured in DMEM supplemented with 10% FCS. A SNAP-tagged HEK293 cell line stably expressing the human SNAP-A_2AR was generated by Dr. Laura Kilpatrick who performed the transfection, dilution cloning and isolation of a stable clone line. HEK293 cells expressing the GloSensor cAMP bionsensor (HEK293G) were obtained from Promega (United States). The HEK293 cell lines were maintained in DMEM containing 10% FCS and 2 mM L-glutamine and were grown to 70-80% confluency in 75cm^2 tissue culture flask before splitting. All cell colonies were incubated at 37 °C, 5% CO_2 and the tissue culture procedures were performed in a class II laminar flow hood using sterile conditions. *Transient Transfection* of NanoLuc-tagged human A_2AR in HEK293G cell line was carried out as follows: 72 h prior the experiment cells were

removed from a confluent T75 flask and centrifuged. The pellet of cells was re-suspended in 10mL of fresh complete DMEM. Afterwards, each CORNING® 10mmx20mm style dish was seeded with a density of $3x10^6$ cells per dish in 10mL complete DMEM. 48 h prior the experiment transfection of the NanoLuc-tagged human A_2AR in HEK 293G cell line was carried out using a mixture of 6 µg DNA and 12 µL FuGENE®(1:2 ratio) in 880 µl OptiMEM, followed by 5 min incubation at room temperature to allow the DNA: FuGENE complex to form. After that time, the entire mixture was carefully added to the CORNING® dish and incubated at 37°C, 5%CO_2 overnight. 24h prior the experiment day cells were removed from a confluent dish and centrifuged. The pellet of cells was re-suspended in 10 mL of fresh DMEM and the resulting NanoLuc-tagged *h*A_2AR HEK293G cells were seeded in white Thermo Scientific 96-well plates at a density of 32000 cells/well and grown in normal growth medium. *Terbium labelling of SNAP-tagged $A_{2A}AR$ cells* To terbium label the SNAP-HEK293-$A_{2A}AR$ cells, cell culture media was removed from confluent SNAP-HEK293-$A_{2A}AR$ cells contained in T175 cm^2 flasks, washed once in DPBS and then incubated with 100nM of SNAP-Lumi4-Tb in 1xLabMed buffer for 1h at 37°C, 5%CO_2. Then the terbium labelling reagent was removed and cells were washed once with ice cold 15 mL PBS. The cells were then removed from the wall of the flask by scraping and centrifuged at 2000 rpm for 10 min and the resulting cell pellets were stored at -80°C. *Membrane preparations of Terbium-labelled SNAP-HEK293-$A_{2A}AR$ cells.* The following described steps were conducted at 4°C to circumvent receptor degradation. Thawed pellets of cells were resuspended in PBS and homogenized using an electronical homogenizer, 10x2 sec bursts. Homogenized solution of cells was centrifuged at 1500 rpm for 20 min to remove unbroken cells and nuclei. The supernatant was subsequently centrifuged at 41,415 g for 30 min. The resulting pellet was resuspended in 4 mL PBS and fully homogenized. Protein concentration was

determined using a BCA protein assay and membranes were stored at -80°C until required. Before their use, frozen membranes were thawed and suspended in HBSS buffer

Experiments

NanoBRET HEK 293 cells were transiently transfected to express Nluc-A_{2A}AR. HEK293 cells expressing Nluc-AR were seeded in white Termo Scientific 96-well plates and grown 24 h prior the day of the experiment in normal growth medium. Before the experiment, DMEM was replaced with HBSS. For saturation and competition assays the required concentration of fluorescent ligands and competing ligand was added at the same time. Thereafter, plates were incubated for 2 h at 37 °C. After 2 h 10 μM furimazine (1:40 dilution; Promega) was added to each well. After 5 min of incubation at 37 °C bioluminescence emission at two different wavelenghts was measured using a PHERAstar FS plate reader (BMG Labtech) at room temperature. The filter light emissions were read at 420nm (80 nm bandpass) and 535 nm (60nm-bandpass) for BYFL-labelled ligands and at 420 nm (80 nm-bandpass) and > 610 nm (longapass) for the BY630/Cy5/AF647-labelled ligands. The raw BRET ratio was calculated by dividing the > 610 nm emission or 533 nm emission by the 420 nm emission. The term "raw BRET ratio" refers to the unprocessed data as no background ratio has been subtracted.

CRE-SPAP assay. 48 h prior the experiment day CHO CRE-SPAP A_2AR cells were seeded onto clear 96-well plates and subsequently serum starved 24 h before the experiment employing DMEM-12 supplemented with 2 mM L-glutamine (serum-free media). On the day of the assay serum-free media was added to the cells and the fluorescent compounds under investigation were further added to the appropriate well at three concentrations (10 nM, 100 nM, 1000 nM), and the plates were incubated for 30 min at 37 °C, 5% CO_2. After 30 min NECA was added at increasing

concentrations and the plates were incubated for further 5h at 37 °C/5% CO_2. Following 5h incubation the media was removed and replaced with 40 μL of serum-free media. The plates were further incubated for 1h at 37 °C/5% CO_2. Following 1h incubation the plates were moved to an oven at 65 °C for 30 min in order to degrade endogenous alkaline phosphatases. The plates were then allowed to cool to room temperature and 100 μL of 5 mM of 4-*p*-nitrophenyl phosphate in DEA buffer (100 nM Diethanolamine; 280 nM NaCl; 0.5 nM $MgCl_2.6H_2O$, pH=9.85) were added in each well and the plates incubated at 37°C for 15 min. Once the yellow color has developed, the plates were read on the Dynex MRX plate reader which measured the absorbance at 405 nm.

*HTRF Binding Kinetic of BODIPY-630/650-X conjugate **12*** To determine the binding kinetics of fluorescent conjugate **12,** HEK293 SNAP-$h$$A_{2A}$AR cell membranes were diluted to the required concentration (10 μg/well) in HBSS buffer containing saponin (1 mg/mL) and added in white Thermo Scientific 96-well microplates. Fluorescent conjugate **12** was added simultaneously at four different concentrations in the presence and absence of 10 μM ZM241385 to define non-specific binding. The plates were read immediately: each well was read every 30 s for 60 min. TR-FRET signals were acquired in a PHERAstarFS plate reader (BMG Labtech) equipped with a Homogeneous Time Resolved Fluorescence module with excitation at 337 nm and emission 620 nm and 655 nm. HTRF ratios were calculated by dividing the acceptor signal (655 nm) by the donor signal (620 nm).

Confocal Microscopy. Cell were grown to 70-80% confluence in eight-well borosilicate chambered-coverglass plates (Nunc Nalgene, Rochester, NY) pre-coated with Poly-D-lysine 48h before imaging. On the day of the experiment medium was removed and the cells were labelled

for 30 min at 37 °C with 0.2 μM SNAP AF488 or AF647 as required in fresh HBSS [HEPES Balanced Salt Solution (HBSS), 25 mM HEPES, 10 mM glucose, 145 mM NaCl, 5 mM KCl, 1 mM $MgSO_4$, 2 mM sodium pyruvate, 1.3 mM $CaCl_2$ at pH 7.4]. After washing twice with HBSS the cells were treated with or without 1 μM ZM241385 for 30 min at 37 °C. Following the incubation step the fluorescent ligands under investigation were added to the appropriate wells at the required concentrations. Live cell imaging was performed at 37 °C using a Zeiss LSM 710 laser scanning confocal microscope fitted with a Zeiss Plan-Neofluar 40 x 1.2 NA water immersion objective. A 633 nm HeNe laser was used for the excitation of the BODIPY630/650, Cy5 and AF647 representative fluorophores and A 488/561/633 dichroic, and the emission was detected using 650 nm LP filter. A 488 nm HeNe laser was used for BODIPY-FL fluorophores series and the emission was detected using LP575 filter. The pinhole diameter (1 Airy Unit; 1.1μm optical slice), laser power and gained remained constant in all the experiments. Images were processed in Zeiss Zen 2 (blue edition) software and linear adjustments to the brightness and contrast have been applied equally across all the images.

Data Analysis. All data are represented as mean ± SEM of n experiments performed in triplicate. The n refers to the number of separate experiments. A separate experiment requires cells plated from a separate flask and separate drug dilution used throughout the experiment. The data is presented and analyzed using Prism software (GraphPad Prism 7) and Excel.

Reporter Gene SPAP Assay: Antagonism by unlabeled and labelled (fluorescent) ligands of the CRE-reporter gene response (SPAP, secreted placental alkaline phosphatase) to NECA in CHO cells expressing the human A_{2A} AR was analyzed. For each concentration of the antagonists, the ratio (DR, dose ratio) of NECA concentrations required to produce the same sized response in

the presence and absence of the antagonist was determined. The antagonist dissociation constant (K_B) was determined by globally fitting the data to the Schild equation:

Schild : $\text{Log (DR-1)} = \text{Log([B])} - \text{Log}K_B$

Where DR (dose ratio) is the ratio of the agonist concentration required to stimulate an identical response in the presence or absence of antagonist, [B]. K_B represents the equilibrium dissociation constant of the antagonist.

NanoBRET Assay: Total and non-specific saturation binding curves were fitted simultaneously using the following equation:

$$\text{BRETratio} = \frac{B\max [\text{B}]}{[B] + (KD)} + \text{M[B]} + \text{C}$$

Where Bmax is the maximal response, [B] is the concentration of fluorescent ligand in nM, K_D is the equilibrium dissociation constant in nM, M is the slope of the nonspecific binding component, and C is the intercept with the y axis.

The competition binding curves were fitted to the following equation:

Uninhibited specific binding = 100 - $\frac{100 \times [A]}{[A] + (IC_{50})}$

Where [A] is the concentration of competing drug and the IC_{50} is the molar concentration of ligand required to inhibit 50% of the specific binding of 50 nM AlexaFluor647-bearing probe **17**.

The Cheng-Prusoff equation was used to correct fitted IC_{50} values to K_i values:

$$K_i = \frac{IC_{50}}{1 + \frac{[L]}{K_D}}$$

Where [L] is the concentration of fluorescent ligand in nM and K_D is the dissociation constant of fluorescent ligand in nM. The calculated K_D values used were as calculated from the saturation binding experiments.

HTRF binding kinetic assay: From Association binding kinetics, non-specific binding was determined for each concentration of the fluorescent conjugate at each time point by adding 10 μM of ZM241385 and this was subtracted from total binding to obtain specific binding measurements. The association rate (k_{on}) in M^{-1} min^{-1} and dissociation rate (k_{off}) in min^{-1} constants were calculated from specific binding following equation:

$$k_{on} = \frac{k_{obs} - k_{off}}{[L]}$$

Where [L] is the concentration of the fluorescent conjugate in M and k_{obs} is calculated from the global fitting of the data to the following exponential association function:

$$Y = Y_{max}(1 - e^{-k_{obs}t})$$

Where Y is the specific binding at time t, Y_{max} represents the specific binding at infinite time (t), and k_{obs} is the rate constant for the observed rate of association.

The kinetic equilibrium dissociation constant (K_D) was determined from the data using the following equation:

$$K_D = \frac{k_{off}}{k_{on}}$$

ASSOCIATED CONTENT

Supporting Information.

The supporting information (SI) is available free of charge on the ACS Publications website at DOI:

Additional pharmacological data and analytical HPLC chromatograms of the final fluorescent ligands. Molecular formula strings of tested compounds (.csv).

AUTHOR INFORMATION

Corresponding Authors

*Barrie Kellam Tel: +44-115-9513026. Fax: +44-115-9513412. E-mail: barrie.kellam@nottingham.ac.uk

*Stephen J. Hill Tel: +44-115-8230082. Fax: +44-115-8230081. E-mail: stephen.hill@nottingham.ac.uk

ORCID

Barrie Kellam: 0000-0003-0030-9908

Stephen J Hill: 0000-0002-4424-239X

Peter J. Scammells: 0000-0003-2930-895X

Leigh A. Stoddart: 0000-0002-4469-0600

Mark Soave: 0000-0002-9199-1772

Eleonora Comeo: 0000-0001-5339-5382

Notes

The authors declare no competing financial interest.

ACKNOWLEDGMENTS

The authors acknowledge the School of Life Sciences Imaging Facility, specifically Tim Self for assistance with the confocal microscopy. The authors also thank the School of Chemistry Mass Spectrometry and NMR services of the University of Nottingham. This work was supported by the Medical Research Council (grant number MR/NO20081/1) and the Nottingham-Monash Joint Doctoral Training Center program.

ABBREVIATIONS

ATP, adenosine 5'-triphospate; AF647, AlexaFluor647; AR, adenosine receptor; BODIPY, 4,4-difluoro-4-bora-3a,4a-diaza-s-indacene; BRET, bioluminescence resonance energy transfer; cAMP, cyclic adenosine monophosphate; CNS, central nervous system; Cy5, cyanine5; DIPEA, diisopropylethylamine; ESI, electrospray ionisation; FCS, fluorescence correlation spectroscopy; FRET; fluorescence resonance energy transfer; GPCR, G protein-coupled receptor; HATU, *O*-(7-azabenzotriazol-1-yl)-1,1,3,3-tetramethyluronium hexafluorophosphate; HEK, human

embryonic kidney; HPLC, high-performance liquid chromatography; HRMS, high-resolution mass spectrometry; LC-MS, liquid chromatography-mass spectrometry; NanoBRET, nanoluciferase-bioluminescence-resonance energy transfer; NanoLuc, nanoluciferase; NMR, nuclear magnetic resonance; RP, reverse-phase; PD, Parkinson's disease; SAR, structure-activity-relationship; SPAP, secreted placental alkaline phosphatase; TR-FRET, time-resolved fluorescence resonance energy transfer.

REFERENCES

(1) Santos, R.; Ursu, O.; Gaulton, A.; Bento, A. P.; Donadi, R. S.; Bologa, C. G.; Karlsson, A.; Al-Lazikani, B.; Hersey, A.; Oprea, T. I.; Overington, J. P. A Comprehensive Map of Molecular Drug Targets. *Nat. Rev. Drug Discov.* **2017**, *16* (1), 19–34.

(2) Fredholm, B. B.; Arslan, G.; Halldner, L.; Kull, B.; Schulte, G.; Wasserman, W. Structure and Function of Adenosine Receptors and Their Genes. *Naunyn. Schmiedebergs. Arch. Pharmacol.* **2000**, *362* (4–5), 364–374.

(3) Ruiz, M. D. L.; Lim, Y.; Zheng, J. Adenosine A2A Receptor as a Drug Discovery Target. *J. Med. Chem.* **2014**, *57* (9), 3623–3650.

(4) Müller, C. E.; Jacobson, K. A. Recent Developments in Adenosine Receptor Ligands and Their Potential as Novel Drugs. *Biochim. Biophys. Acta - Biomembr.* **2011**, *1808* (5), 1290–1308.

(5) Kull, B.; Svenningsson, P.; Fredholm, B. B. Adenosine A(2A) Receptors Are Colocalized with and Activate g(Olf) in Rat Striatum. *Mol. Pharmacol.* **2000**, *58* (4), 771–777.

(6) Fredholm, B. B.; IJzerman, A. P.; Jacobson, K. A; Klotz, K. N.; Linden, J. International Union of Pharmacology. XXV. Nomenclature and Classification of Adenosine Receptors. *Pharmacol. Rev.* **2001**, *53* (4), 527–552.

(7) Jaakola, V.P.; Griffith, M.T.; Hanson, M.A.; Cherezov, V.; Chien, E.Y.; Lane, J.R.; Ijzerman, A.P;, Stevens, R.C. The 2.6 Angstrom Crystal Structure of a Human A_{2A} Adenosine Receptor Bound to an Antagonist. *Science* **2008**, *322* (2), 1211–1218.

(8) Xu, F.; Wu, H.; Katritch, V.; Han, G. W.; Jacobson, K. A.; Gao, Z.-G.; Cherezov, V.; Stevens, R. C. Structure of an Agonist-Bound Human A_{2A} Adenosine Receptor. *Science* **2011**, *332* (6027) , 322–327

(9) Liu, W.; Chun, E.; Thompson, A. A.; Chubukov, P.; Xu, F.; Han, G. W.; Roth, C. B.; Heitman, L. H.; Ijzerman, A. P.; Cherezov, V.; Stevens, R. C. Structural Basis for Allosteric Regulation of GPCRs by Sodium Ions. *Science* **2013**, *337* (6091), 232–236.

(10) Langmead, C. J.; Andrews, S. P.; Congreve, M.; Errey, J. C.; Hurrell, E.; Marshall, F. H.; Mason, J. S.; Richardson, C. M.; Robertson, N.; Zhukov, A.; Weir, M. Identification of Novel Adenosine A $_{2A}$ Receptor Antagonists by Virtual Screening. *J. Med. Chem.* **2012**, *55* (5), 1904–1909.

(11) Congreve, M.; Andrews, S. P.; Doré, A. S.; Hollenstein, K.; Hurrell, E.; Langmead, C. J.; Mason, J. S.; Ng, I. W.; Tehan, B.; Zhukov, A.; Weir, M.; Marshall, F. H. Discovery of 1,2,4-Triazine Derivatives as Adenosine A2Aantagonists Using Structure Based Drug Design. *J. Med. Chem.* **2012**, *55* (5), 1898–1903.

(12) Jacobson, K. A. and Gao, Z.-G. Adenosine Receptors as Therapeutic Targets. *Nat. Rev. Drug Discov.* **2006**, *49* (5), 247–264.

(13) Chen, J.-F.; Eltzschig, H. K.; Fredholm, B. B. Adenosine Receptors as Drug Targets — What Are the Challenges? *Nat. Rev. Drug. Discov.* **2013**, *12* (4), 265–286.

(14) Burnstock, G. Purinergic Signalling and Disorders of the Central Nervous System. *Nat. Rev. Drug Discov.* **2008**, *7* (7), 575–590.

(15) Antonioli, L.; Blandizzi, C.; Pacher, P.; Haskó, G. Immunity, Inflammation and Cancer: A Leading Role for Adenosine. *Nat. Rev. Cancer* **2013**, *13* (12), 842–857.

(16) Ohta, A.; Gorelik, E.; Prasad, S. J.; Ronchese, F.; Lukashev, D.; Wong, M. K. K.; Huang, X.; Caldwell, S.; Liu, K.; Smith, P.; Chen, J-F.; Jackson, E. K.; Apasov, S.; Abrams, S.; Sitkovsky, M. A_{2A} Adenosine Receptor Protects Tumors from Antitumor T Cells. *Proc. Natl. Acad. Sci. USA.* **2006**, *103* (35), 13132–13137.

(17) Ohta, A. A Metabolic Immune Checkpoint: Adenosine in Tumor Microenvironment. *Front. Immunol.* **2016**, *7*, 109.

(18) Inoue, Y.; Yoshimura, K.; Kurabe, N.; Kahyo, T.; Kawase, A.; Tanahashi, M.; Ogawa, H.; Inui, N.; Funai, K.; Shinmura, K.; Niwa, H.; Suda, T.; Sugimura, H. Prognostic Impact of CD73 and A2A Adenosine Receptor Expression in Non-Small-Cell Lung Cancer. *Oncotarget* **2017**, *8* (5), 8738–8751.

(19) Al Jaroudi, W.; Iskandrian, A. E. Regadenoson: A New Myocardial Stress Agent. *J. Am. Coll. Cardiol.* **2009**, *54* (13), 1123–1130.

(20) Dungo, R.; Deeks, E. D. Istradefylline: First Global Approval. *Drugs* **2013**, *73* (8), 875-882.

(21) U. S. Food and Drug Administration. FDA approves new add-on drug to treat off episodes in adults with Parkinson's disease https://www.fda.gov/news-events/press-announcements/fda-approves-new-add-drug-treat-episodes-adults-parkinsons-disease.

(22) Arruda, M. A.; Stoddart, L. A.; Gherbi, K.; Briddon, S. J.; Kellam, B.; Hill, S. J. A Non-Imaging High Throughput Approach to Chemical Library Screening at the Unmodified Adenosine-A_3 Receptor in Living Cells. *Front. Pharmacol.* **2017**, *8,* 908.

(23) Vernall, A. J.; Stoddart, L. A.; Briddon, S. J.; Hill, S. J.; Kellam, B. Highly Potent and Selective Fluorescent Antagonists of the Human Adenosine A3 Receptor Based on the 1,2,4-Triazolo[4,3-a]Quinoxalin- 1-One Scaffold. *J. Med. Chem.* **2012**, *55* (4), 1771–1782.

(24) Stoddart, L. A.; Vernall, A. J.; Briddon, S. J.; Kellam, B.; Hill, S. J. Direct Visualisation of Internalization of the Adenosine A3 Receptor and Localization with Arrestin3 Using a Fluorescent Agonist. *Neuropharmacology* **2015**, *98*, 68–77.

(25) Middleton, R. J.; Briddon, S. J.; Cordeaux, Y.; Yates, A. S.; Dale, C. L.; George, M. W.; Baker, J. G.; Hill, S. J.; Kellam, B. New Fluorescent Adenosine A_1-Receptor Agonists That Allow Quantification of Ligand - Receptor Interactions in Microdomains of Single Living Cells. *J. Med. Chem.* **2007**, *50* (4), 782–793.

(26) Briddon, S. J.; Middleton, R. J.; Cordeaux, Y.; Flavin, F. M.; Weinstein, J. A.; George, M. W.; Kellam, B.; Hill, S. J. Quantitative Analysis of the Formation and Diffusion of A1-

Adenosine Receptor – Antagonist Complexes in Single Living Cells. *PNAS* **2004**, *101* (13), 4673–4678.

(27) Kecskés, M.; Kumar, T. S.; Yoo, L.; Gao, Z. G.; Jacobson, K. A. Novel Alexa Fluor-488 Labeled Antagonist of the A2A Adenosine Receptor: Application to a Fluorescence Polarization-Based Receptor Binding Assay. *Biochem. Pharmacol.* **2010**, *80* (4), 506–511.

(28) Duroux, R.; Ciancetta, A.; Mannes, P.; Yu, J.; Boyapati, S.; Gizewski, E.; Yous, S.; Ciruela, F.; Auchampach, J. A.; Gao, Z.-G.; Jacobson, K. A. Bitopic Fluorescent Antagonists of the A_{2A} Adenosine Receptor Based on Pyrazolo[4,3-e][1,2,4]Triazolo[1,5-c]Pyrimidin-5-Amine Functionalized Congeners. *Med. Chem. Commun.* **2017**, *8* (8), 1659–1667.

(29) Neustadt, B. R.; Hao, J.; Lindo, N.; Greenlee, W. J.; Stamford, A. W.; Tulshian, D.; Ongini, E.; Hunter, J.; Monopoli, A.; Bertorelli, R.; Foster, C.; Arik, L.; Lachowicz, J.; Ng, K.; Feng, K. I. Potent, Selective, and Orally Active Adenosine A2Areceptor Antagonists: Arylpiperazine Derivatives of Pyrazolo[4,3-e]-1,2,4-Triazolo[1,5-c]Pyrimidines. *Bioorg. Med. Chem. Lett.* **2007**, *17* (5), 1376–1380.

(30) Shinkre, B. A.; Kumar, T. S.; Gao, Z. G.; Deflorian, F.; Jacobson, K. A.; Trenkle, W. C. Synthesis and Evaluation of 1,2,4-Triazolo[1,5-c]Pyrimidine Derivatives as A_{2A} Receptor-Selective Antagonists. *Bioorganic Med. Chem. Lett.* **2010**, *20* (19), 5690–5694.

(31) Basu, S.; Barawkar, D. A.; Ramdas, V.; Naykodi, M.; Shejul, Y. D.; Patel, M.; Thorat, S.; Panmand, A.; Kashinath, K.; Bonagiri, R.; Prasad, V.; Bhat, G.; Quraishi, A.; Chaudhary, S.; Magdum, A.; Meru, A. V.; Ghosh, I.; Bhamidipati, R. K.; Raje, A. A.; Madgula, V. L. M.; De, S.; Rouduri, S. R.; Palle, V. P.; Chugh, A.; Hariharan, N.; Mookhtiar, K. A. Discovery of Potent

and Selective A_{2A} Antagonists with Efficacy in Animal Models of Parkinson's Disease and Depression. *ACS Med. Chem. Lett.* **2017**, *8* (8), 835–840.

(32) Carlsson, J.; Yoo, L.; Gao, Z.-G.; Irwin, J. J.; Shoichet, B. K.; Jacobson, K. A. Structure-Based Discovery of A_{2A} Adenosine Receptor Ligands. *J. Med. Chem.* **2010**, *53* (9), 3748–3755.

(33) Baraldi, S.; Baraldi, P. G.; Oliva, P.; Toti, K. S.; Ciancetta, A.; Jacobson, K. A. A_{2A} Adenosine Receptor : Structures, Modeling, and Medicinal Chemistry; *The Adenosine Receptors.* **2018**, *34*, 91-136.

(34) Baker, J. G.; Middleton, R.; Adams, L.; May, L. T.; Briddon, S. J.; Kellam, B.; Hill, S. J. Influence of Fluorophore and Linker Composition on the Pharmacology of Fluorescent Adenosine A_1 Receptor Ligands: Themed Section: Imaging in Pharmacology Research Paper. *Br. J. Pharmacol.* **2010**, *159* (4), 772–786.

(35) Vernall, A. J.; Stoddart, L. A.; Briddon, S. J.; Ng, H. W.; Laughton, C. A.; Doughty, S. W.; Hill, S. J.; Kellam, B. Conversion of a Non-Selective Adenosine Receptor Antagonist into A_3-Selective High Affinity Fluorescent Probes Using Peptide-Based Linkers. *Org. Biomol. Chem.* **2013**, *11* (34), 5673.

(36) Stoddart, L. A.; Vernall, A. J.; Bouzo-Lorenzo, M.; Bosma, R.; Kooistra, A. J.; De Graaf, C.; Vischer, H. F.; Leurs, R.; Briddon, S. J.; Kellam, B.; Hill, S. J. Development of Novel Fluorescent Histamine H1-Receptor Antagonists to Study Ligand-Binding Kinetics in Living Cells. *Sci. Rep.* **2018**, *8* (1), 1–19.

(37) Conroy, S.; Kindon, N. D.; Glenn, J.; Stoddart, L. A.; Lewis, R. J.; Hill, S. J.; Kellam, B.; Stocks, M. J. Synthesis and Evaluation of the First Fluorescent Antagonists of the Human $P2Y_2$ Receptor Based on AR-C118925. *J. Med. Chem.* **2018**, *61* (7), 3089-3113.

(38) Schembri, L. S.; Stoddart, L. A.; Briddon, S. J.; Kellam, B.; Canals, M.; Graham, B.; Scammells, P. J. Synthesis, Biological Evaluation, and Utility of Fluorescent Ligands Targeting the μ-Opioid Receptor. *J. Med. Chem.* **2015**, *58* (24), 9754–9767.

(39) Ulrich, G.; Ziessel, R.; Harriman, A. The Chemistry of Fluorescent Bodipy Dyes: Versatility Unsurpassed. *Angew. Chem. Int. Ed.* **2008**, *47* (7), 1184–1201.

(40) Alcobia, D. C.; Ziegler, A. I.; Kondrashov, A.; Comeo, E.; Mistry, S.; Kellam, B.; Chang, A.; Woolard, J.; Hill, S. J.; Sloan, E. K. Visualising Ligand-Binding to a GPCR in Vivo Using NanoBRET. *iScience* **2018**, *6*, 280–288.

(41) Saccomano, M.; Dullin, C.; Alves, F.; Napp, J. Preclinical Evaluation of Near-Infrared (NIR) Fluorescently Labeled Cetuximab as a Potential Tool for Fluorescence-Guided Surgery. *Int. J. Cancer* **2016**, *139* (10), 2277–2289.

(42) Kuo, Shen-Chun; Tran, Thanh; Zhang, P. Process For Preparing Substituted 5-Amino-pyrazolo-[4,3-*e*]- 1,2,4-triazolo[1,5-*c*]pyrimidine. U.S. Patent 7,235,659, Jun 26, 2007.

(43) Klötzer, W; Herberz, M. Chlorierende Formylierungsreaktionen an Pyrimidinen Die Reaktion Des Formylierungsreagens Mit Einer Am Pyrimidinkern. *Monatsh. Chem.* **1965**, *96* (5), 1567–1572.

(44) Ashry, E. S. H. E. L.; Rashed, Y. E. L. K. N.; Assafir, H. Dimroth Rearrangement : Translocation of Heteroatoms in Heterocyclic Rings and Its Role in Ring Transformations of Heterocycles. *Adv. Heterocycl. Chem.* **1999**, *75*, 79–165.

(45) Dale, C. L.; Hill, S. J.; Kellam, B. New Potent, Short-Linker BODIPY-630/650™ Labelled Fluorescent Adenosine Receptor Agonists. *Med. Chem. Commun.* **2012**, *3* , 333–338.

(46) Stoddart, L. A.; Kilpatrick, L. E.; Hill, S. J. NanoBRET Approaches to Study Ligand Binding to GPCRs and RTKs. *Trends Pharmacol. Sci.* **2018**, *39* (2), 136–147.

(47) Dale, N. C.; Johnstone, E. K. M.; White, C. W.; Pfleger, K. D. G. NanoBRET: The Bright Future of Proximity-Based Assays. *Front. Bioeng. Biotechnol.* **2019**, *7*, 56.

(48) Hall, M. P.; Unch, J.; Binkowski, B. F.; Valley, M. P.; Butler, B. L.; Wood, M. G.; Otto, P.; Zimmerman, K.; Vidugiris, G.; Machleidt, T.; Robers, M. B.; Benink, H. A.; Eggers, C. T.; Slater, M. R.; Meisenheimer, P. L.; Klaubert, D. H.; Fan, F.; Encell, L. P.; Wood, K. V. Engineered Luciferase Reporter from a Deep Sea Shrimp Utilizing a Novel Imidazopyrazinone Substrate. *ACS Chem. Biol.* **2012**, *7* (11), 1848–1857.

(49) Machleidt, T.; Woodroofe, C. C.; Schwinn, M. K.; Méndez, J.; Robers, M. B.; Zimmerman, K.; Otto, P.; Daniels, D. L.; Kirkland, T. A.; Wood, K. V. NanoBRET-A Novel BRET Platform for the Analysis of Protein-Protein Interactions. *ACS Chem. Biol.* **2015**, *10* (8), 1797–1804.

(50) Hill, S. J.; Baker, J. G.; Rees, S. Reporter-Gene Systems for the Study of G-Protein-Coupled Receptors. *Curr. Opin. Pharmacol.* **2001**, *1* (5), 526–532.

(51) Christopoulos, A.; Kenakin, T. G Protein-Coupled Receptor Allosterism and Complexing. *Pharmacol. Rev.* **2002**, *54* (2), 323–374.

(52) Sykes, D. A.; Stoddart, L. A.; Kilpatrick, L. E.; Hill, S. J. Binding Kinetics of Ligands Acting at GPCRs. *Mol. Cell. Endocrinol.* **2019**, *485*, 9–19.

(53) Copeland, R. A.; Pompliano, D. L.; Meek, T. D. Drug – Target Residence Time and Its Implications for Lead Optimization. *Nat. Rev. Drug Discov.* **2007**, *5*, 730–740.

(54) Guo, D.; Heitman, L. H.; Ijzerman, A. P. Kinetic Aspects of the Interaction between Ligand and g Proteincoupled Receptor: The Case of the Adenosine Receptors. *Chem. Rev.* **2017**, *117* (1), 38–66.

(55) Stoddart, L. A.; Kilpatrick, L. E.; Briddon, S. J.; Hill, S. J. Probing the Pharmacology of G Protein-Coupled Receptors with Fluorescent Ligands. *Neuropharmacology* **2015**, *98*, 48–57.

(56) Stoddart, L. A.; White, C. W.; Nguyen, K.; Hill, S. J.; Pfleger, K. D. G. Fluorescence- and Bioluminescence-Based Approaches to Study GPCR Ligand Binding. *Br. J. Pharmacol.* **2016**, *173* (20), 3028–3037.

(57) Sykes, D. A.; Moore, H.; Stott, L.; Holliday, N.; Javitch, J. A.; Lane, J. R.; Charlton, S. J. Extrapyramidal Side Effects of Antipsychotics Are Linked to Their Association Kinetics at Dopamine D2 Receptors. *Nat. Commun.* **2017**, *8* (763), 1–11.

(58) Cottet, M.; Faklaris, O.; Maurel, D.; Scholler, P.; Doumazane, E.; Trinquet, E.; Pin, J. P.; Durroux, T. BRET and Time-Resolved FRET Strategy to Study GPCR Oligomerization: From Cell Lines toward Native Tissues. *Front. Endocrinol.* **2012**, *3*, 92.

(59) Fredholm, B. B.; IJzerman, A. P.; Jacobson, K. A.; Linden, J.; Müller, C. E. International Union of Pharmacology. LXXXI. Nomenclature and Classification of Adenosine Receptors-An Update. *Pharmacol Rev* **2011**, *63* (1), 1–34.

(60) Ongini, E.; Dionisotti, S.; Gessi, S.; Irenius, E.; Fredholm, B. B. Comparison of CGS 15943, ZM 241385 and SCH 58261 as Antagonists at Human Adenosine Receptors. *Naunyn. Schmiedebergs. Arch. Pharmacol.* **1999**, *359* (1), 7–10.

(61) Bunnage, M. E.; Chekler, E. L. P.; Jones, L. H. Target Validation Using Chemical Probes. *Nat. Chem. Biol.* **2013**, *9* (4), 195–199.

(62) Simon, G. M.; Niphakis, M. J.; Cravatt, B. F. Determining Target Engagement in Living Systems. *Nat. Chem. Biol.* **2013**, *9* (4), 200–205.

(63) Stoddart, L. A.; Johnstone, E. K. M.; Wheal, A. J.; Goulding, J.; Robers, M. B.; MacHleidt, T.; Wood, K. V.; Hill, S. J.; Pfleger, K. D. G. Application of BRET to Monitor Ligand Binding to GPCRs. *Nat. Methods* **2015**, *12* (7), 661–663.

TABLE OF CONTENT GRAPHIC

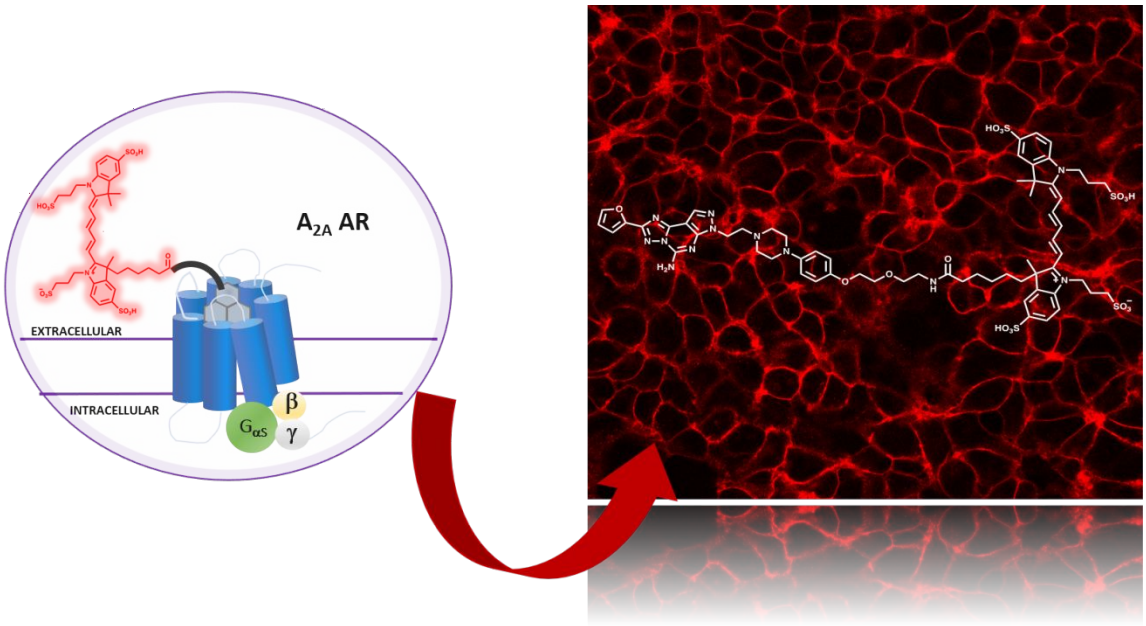
A2A AR
EXTRACELLULAR
INTRACELLULAR
Gαs
β
γ